SUB-CYTOTOXIC NANOPARTICLE EXPOSURE TO AIRWAY EPITHELIAL CELLS CAUSES ALTERATIONS IN CELLULAR SIGNALING

by

Mia McCorkel

A Thesis Submitted to the Faculty of the

GRADUATE INTERDISCIPLINARY PROGRAM IN
BIOMEDICAL ENGINEERING

In Partial Fulfillment of the Requirements
For the Degree of

MASTER OF SCIENCE

In the Graduate College
THE UNIVERSITY OF ARIZONA

2011

STATEMENT BY AUTHOR

This thesis has been submitted in partial fulfillment of requirements for an advanced degree at The University of Arizona and is deposited in the University Library to be made available to borrowers under rules of the Library.

Brief quotations from this thesis are allowable without special permission, provided that accurate acknowledgment of source is made. Requests for permission for extended quotation from or reproduction of this manuscript in whole or in part may be granted by the head of the major department or the Dean of the Graduate College when in his or her judgment the proposed use of the material is in the interests of scholarship. In all other instances, however, permission must be obtained from the author.

SIGNED: _____
Mia McCorkel

APPROVAL BY THESIS DIRECTOR
This thesis has been approved on the date shown below:

_____ 5.12.11
Scott Boitano Date
Professor of Physiology

ACKNOWLEDGEMENTS

I thank my advisor Dr. Scott Boitano for his support and mentoring during my graduate studies. His academic guidance has been key in my recent achievements.

I could not be here today without the unconditional love of my family. I hope they know just how much their constant understanding and encouragement means to me.

A special thank you to Christopher Lewis for his loving support, no matter the distance.

I thank the current members of the Boitano Lab: Andrea Flynn, Cara Sherwood, Justin Hoffman, and Bianca Barcelo. It has been a pleasure and an honor to be a part of the group. I especially thank Andrea Flynn for her valuable advice towards this work.

I thank Antonia Luna and Lila Otero Gonzalez for their contributions to this work.

I thank Dr. Reyes Sierra-Alvarez, Dr. Marty Pagel, and Dr. Ron Lynch for their efforts as members of my thesis committee.

TABLE OF CONTENTS

TABLE OF CONTENTS - *continued*

LIST OF FIGURES

LIST OF FIGURES - *continued*

LIST OF TABLES

ABSTRACT

There are strong correlations between ultrafine particle deposition in the lung and chronic respiratory illness. The growing prevalence of engineered nanoparticles (ENPs) in society presents a new lung toxicant exposure that has the potential to cause adverse affects in the lung, and specifically, on lung innate immune function. We examined the cytotoxicity of hafnium oxide (HfO_2), cerium oxide (CeO_2), and silicon oxide (SiO_2) ENPs, and their micron-sized equivalents, to cultured human airway epithelial cells (16HBE14o-) in terms of cell death and reduction in paracrine ATP signaling as a measure of one aspect of innate immune function in lung epithelium. We used high-throughput real time cell analysis (RTCA) assays and fluorescent-based Live/Dead assays to evaluate cell death to establish cytotoxic levels of ENPs to airway epithelium. We used RTCA with digital imaging video microscopy to evaluate changes in ATP-induced cell signaling following exposure to low, non-cytotoxic doses of ENPs (10 – 50 mg/L). ENP induced cytotoxicity occurred only at high exposures, whereas acute (24 hr) incubations with ENPs resulted in altered ATP-induced cellular signaling at low doses of ENPs. We conclude that sub-cytotoxic exposures to ENPs can alter a basic innate immune function in lung epithelial cells that could contribute to respiratory disease. Such measurements of toxicity may be better indicators of potential health hazards of ENPs than simple cell death assays.

CHAPTER 1 - BACKGROUND AND LITERATURE REVIEW

1.1 Introduction

Engineered nanoparticles (ENPs) are intentionally produced structures with diameters less than 100 nm that confer physicochemical properties that differ from their bulk counterparts (Auffan et al., 2009; Gwinn, 2006). They can be composed of pure metals, metal oxides and sulfides, alloys, or various compounds (Karakoti et al., 2011), but their unique physicochemical properties are a function of their small size, chemical composition, surface structure, solubility, shape, and aggregation (Nel et al., 2006). Nanotechnology that incorporates the use of ENPs is transforming established fields such as medical diagnostics, energy conversion, and microelectronics. These fields are rapidly expanding and introducing new applications within areas of molecular electronics, drug design and delivery, and imaging and diagnostic systems. Nanoparticles are increasingly being used for commercial and industrial purposes including semiconductors, fillers, catalysts, biosensors, and cosmetics. Although these applications are being exploited for new nanotechnologies and potential human health benefits, they raise concerns for human health risks due to their possible negative effects on biological systems, acting at the cellular, subcellular, and protein levels.

1.2 Engineered Nanoparticles (ENPs)

The use of nanotechnology in the field of medicine introduces many applications of ENPs. They are used as probes in imaging and diagnosis and can be linked to peptides, antibodies, or nucleic acids to detect products of cellular reactions (Gwinn, 2006). Nanoparticles that act as drug carrying vehicles to target specific sites are improving drug delivery systems. Although this advancing field of nanomedicine has many potential benefits, these applications directly and purposely expose humans to ENPs, which may carry negative health effects as well. Such risks have largely gone without appropriate evaluation.

Exposure to ENPs is widespread other industries as well, where ENPs are used in the production of commercial goods and advanced electronics. ENPs are increasingly used for fillers, opacifiers, catalysts, semiconductors, cosmetics, pigments, fuel additives, polishing agents, UV absorbers, self-cleaning surface coatings, stain-resistant textiles, and microelectronics (Nel et al., 2006; Oberdorster et al., 2005; Xia et al., 2008). They are used in optical sensors based on metal nanoparticle arrays and single nanoparticles with properties that scatter light with remarkable efficiency (plasmonic) to detect molecular binding events and changes in molecular conformation (Anker et al., 2008). Gas and humidity sensors also utilize metal nanoparticle thin films, due to their ability to act as reactive sites to target specific gas molecules (Beliatis et al., 2011). Semiconductor manufacturing incorporates dispersions of nanoparticles as high

refractive index fluids in immersion lithography (Bremer et al., 2009). Colloidal lithography with silver nanoparticles has been used to fabricate nanostructure arrays for optics and optoelectronic purposes, such as for photovoltaic cells, light-emitting devices, and photo-detectors (Park et al., 2010). These uses of ENPs, and many more to follow, increase risk for unintentional exposure.

1.2.1 Types of ENPs

ENP materials used in a wide range of industry and research field are all associated with different physical, chemical, and toxicological properties. ENPs defined by their core composition can be grouped as either organic or inorganic (Ju-Nam and Lead, 2008; Peralta-Videa et al., 2011). Organic, or carbon-based, ENPs include fullerenes (C_{60} and C_{70}) and carbon nanotubes. Inorganic ENPs include those based on metal oxides, metals, semiconductors, or quantum dots. Inorganic ENPs are becoming more prevalent in biomedical applications. In addition to carrying an active drug, they can act as diagnostic agents for spectroscopy or imaging (e.g. by using fluorescent tags or magnetic contrast agents). For successful therapeutic and drug delivery application, it is necessary to protect the surface of the ENP from agglomeration and clearing from the body. Surface modifications of the ENPs, such as the addition functional groups, can alter surface charge, biocompatibility, and solubility of the ENP. One promising functional group is the polymer Poly(ethylene glycol), which when attached to or coated on the ENP surface (i.e. PEGylation), has been found to be effective in

shielding the surface charge of ENPs and can improve the biomedical properties for use in a biological environment (Karakoti et al., 2011).

Metal oxide ENPs are used in biological sciences, as well as in food, material, and chemical applications. Metal oxide ENPs like TiO_2, Fe_2O_3, and ZnO are used in cosmetics and sunscreens. SiO_2 has been used in dental fillings and CeO_2 is used in fuel additives (Ju-Nam and Lead, 2008). HfO_2, with its high dielectric constant, is a promising material for replacing SiO_2 as the gate insulator in complementary metal-oxide semiconductor technology (Ceresoli, 2006). HfO_2 nanoparticles are also applied in immersion lithography to create high refractive index fluids, with can extend the resolution of conventional lithography for transfer of patterns to thin films in deep submicron range (Bremer et al., 2009). During the production processes of these ENP applications, particles are released into the process fluids and potentially work space. Consequently, occupational exposure and ENP emissions may result through the waste streams into the surrounding environment.

1.3 Exposure Routes of Engineered Nanoparticles

Human exposure to ENPs can occur in both occupational (e.g. manufacturing of nanomaterials) and medicinal (e.g. administered as pharmaceuticals) settings. Furthermore, as more ENPs are produced, their increased persistence in the environment will allow for re-entry into biological systems. Once in the body, ENP translocation, cellular uptake, accumulation

and retention, cellular and protein interactions, and potential adverse effects can be influenced by the physicochemical characteristics of the surface and core of the ENP (Nel et al., 2009; Oberdorster et al., 2005).

Because of the size of nanoparticles, they are easily dispersed into the air in their native form in or in complex aerosols, making the lungs a potential target for airborne ENPs, possibly settling on the airway or alveolar epithelium. Particles that translocate over the alveolar epithelium may reach the interstitium or even enter the vascular circulation via the capillary endothelium (Muhlfeld et al., 2008). Another potential route of entry for ENPs is the skin, the largest organ of the body. Here, ENPs may become lodged within the avascular epidermis where they are protected from removal by phagocytosis (Oberdorster et al., 2005). Although it is not addressed in these studies, the gastrointestinal tract is another portal of entry for ENP exposure, via oral ingestion. ENPs may be translocated through the mucosal lining and epithelial barrier of the intestine and enter the circulatory system within only one hour (Muhlfeld et al., 2008).

1.3.1 Risks and Concerns of Engineered Nanoparticles

Despite the many benefits and technological advances that have resulted from use of ENPs, there are potential health and environmental risks that should be considered. Similar to particulate matter originating from combustion-generated ultrafine particles, ENPs that are intentionally manufactured can cause human toxicity effects and negatively impact the environment.

Concern over air pollution in the United States in the 1980s led to many studies on particulate matter originating from smoke, fumes, soot, and combustion by-products, mostly coming from exhaust stacks and tailpipes, but also secondary particles produced from condensation of vaporized materials or oxidation of atmospheric gases. These studies found that the smaller "inhalable particles" were of greatest concern, and thus were focused on particulate matter < 10 μm in aerodynamic diameter (PM_{10}), or < 2.5 μm in diameter ($PM_{2.5}$). Increased mortality and morbidity (both cardiovascular and respiratory) has been associated with particulate air pollution, even at moderate concentrations (Dockery and Pope, 1994). Furthermore, exposure to PM_{10} has been linked to reductions in lung function development (Horak et al., 2002) and increased hospital admissions in patients with chronic obstructive pulmonary disease (COPD), as well as asthma (Samoli et al., 2011) and atherosclerosis (Grahame and Schlesinger, 2010).

The mechanisms for the adverse health effects linked to PM_{10} exposure are not well understood. One hypothesis is that PM_{10} particles cause oxidant stress that results in inflammation and injury to the airway epithelium. This hypothesis has been tested by investigating the effects of intratracheal instillation of PM_{10} in rat lungs (Li et al., 1997). A measured influx of neutrophils in the alveolar space indicated a significant inflammatory response, and an increased epithelial permeability indicated injury to the airway epithelium. Furthermore, when ultrafine carbon black particles (ufCB), composed entirely of ~20 nm

diameter particles, were compared to the larger PM_{10} particles, the smaller ufCB was found to have an even greater inflammatory response compared to PM_{10}. This result showed that smaller particles have the potential to cause greater effects than larger particles.

While ENPs can be similar in size to the incidental nanoparticles produced from air pollution, they are different because ENPs have unique physical and chemical properties that relate to their product applications. These ENPs, which are smaller than 100 nm in at least one dimension, create another source for human exposure to nano-sized particles and may have similar toxicological potentials and biological behavior as the particulate matter of air pollution (Fadeel and Garcia-Bennett, 2010). Therefore, previous studies focused on the adverse health effects of air pollution are relevant starting points from which to study ENPs. With humans purposely exposed to a wide range of ENPs for medical purposes and unintentionally exposed in manufacturing and occupational environments, it is important to carefully assess the toxicology of emerging ENPs, as well as their interactions with biological systems.

1.3.2 Lung structure and its effect on ENP exposure and deposition

The lung can be divided into two functional compartments: the conducting zone made up of airways (trachea, bronchi, and bronchioles) and the respiratory zone lined with alveoli where gas is exchanged. The pseudostratified epithelium lining the airways features ciliated and non-ciliated columnar cells, and

interdispersed goblet cells among a variety of other cell types (Figure 1.1). Together with the submucosal glands, the goblet cells secrete mucus onto the epithelial surface, forming a blanket over the tops of the ciliated cells. This airway surface liquid (ASL) is composed of two layers that aid in ciliary movement that powers foreign material up and out of the lungs. The thick mucus layer of the ASL acts to bind and trap inhaled particles, and the underlying periciliary layer, which is less viscous, allows the cilia to move and push the mucus up the respiratory tract. Proper innate immune function of the conducting airway depends on this mucociliary escalator to clear the ASL containing inhaled particulate matter.

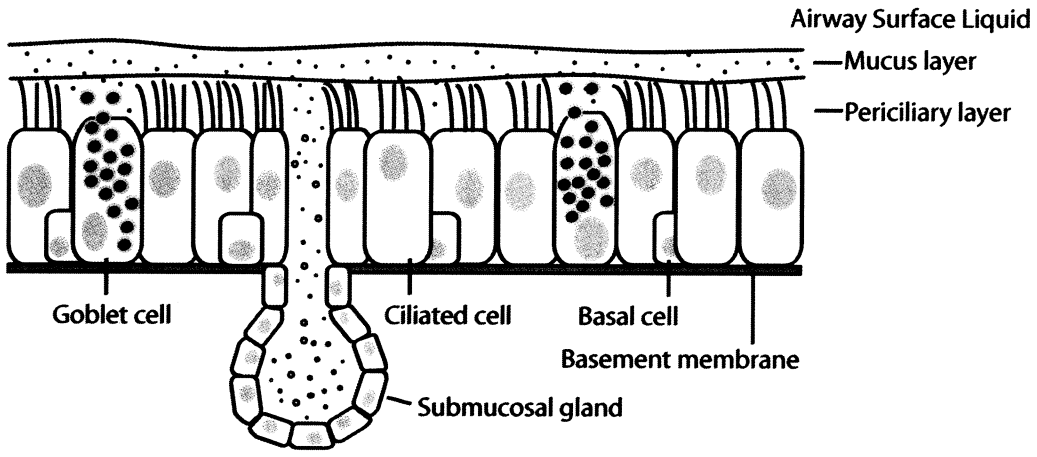

Figure 1.1: Epithelium of the conducting airway. The conducting airway epithelium is composed primarily of ciliated cells and mucus-producing goblet cells. Inhaled particulates are entrapped in the airway surface liquid produced by the goblet cells and submucosal glands. Coordinated ciliary movement propels the airway surface liquid out of the airway. This mucociliary escalator is responsible for particle clearance in the conducting airways. Adapted from (Leff and Schumacker, 1993).

With about 10,000 – 30,000 L of air breathed in per day, the lungs and airways are unavoidably exposed to particulate matter in addition to the oxygen and other gases in the atmosphere. The deposition of smaller particles like ENPs occurs in all regions of the respiratory system and depends on their size, shape, and ventilation parameters (Marijnissen and Gradoń, 2010). Particle diameter is a primary factor in determining the mechanism of pulmonary deposition in the different regions of the respiratory tract, with smaller particles deposited in the smaller airways and alveoli as opposed to the larger airways (Carvalho et al., 2011). Other factors including solubility and viscosity of the material can alter this distribution.

Particle deposition in the lungs occurs by impaction, sedimentation, and diffusion (Figure 1.2A) (Carvalho et al., 2011). The first mechanism of deposition, impaction, increases with particle size and air velocity, and is most influential in the head or extrathoracic region, where large particles travel at high velocities and tend to impact the respiratory tract. Particles deposited due to sedimentation are influenced mostly by gravity. This type of deposition increases with particle size and decreases with air velocity. Therefore, sedimentation is most prominent in the smaller airways and the alveoli (Nordberg et al., 2007). Deposition by diffusion occurs when particles are small enough to undergo random motion due to air molecules interacting with the inhaled and exhaled air, and has most effect when particles are nano-sized (smaller than 100 nm) (Marijnissen and Gradoń, 2010). As particle size decreases to submicron

dimensions, the total lung deposition is also decreased (Figure 1.2B). However, if particle size reaches nanometer diameters, total lung deposition quickly increases back to levels equal to or greater than deposition levels of micron-sized particles (Carvalho et al., 2011).

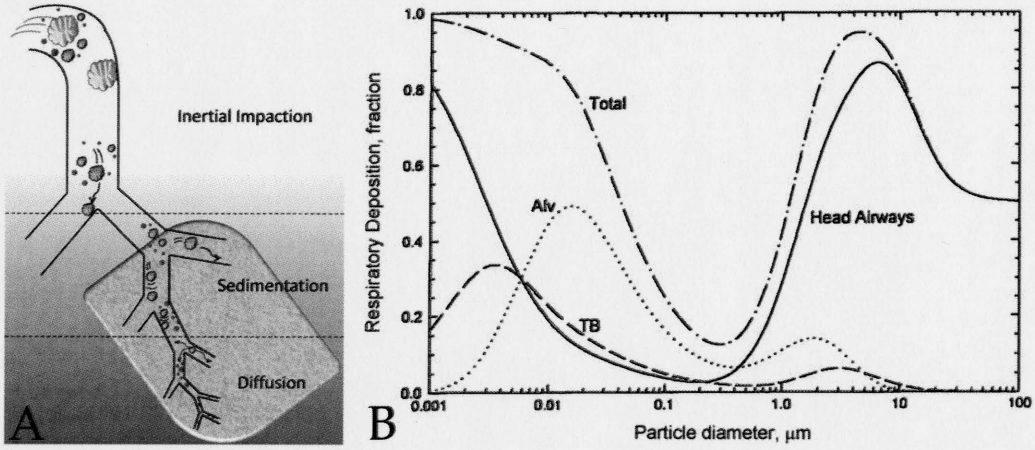

Figure 1.2: Particle deposition in the lungs depends on particle diameter. (A) Particles are deposited by different mechanisms (inertial impaction, sedimentation, or diffusion) depending on particle size. Smaller particles tend to deposit in the lower airways. (B) Average predicted total and regional lung deposition based on International Commission on Radiological Protection (ICRP) deposition model. Alv: alveolar region; TB: tracheobronchial region. Reprinted from International Journal of Pharmaceutics, 406(1-2), T.C. Carvalho, J.I. Peters, R.O. Williams III, Influence of particle size on regional lung deposition – What evidence is there?, pgs. 1-10, Copyright 2011, with permission from Elsevier.

Direct studies to examine the effects of ENP inhalation provide severe difficulties. However, interaction between epithelial cells and ENPs can be modeled in the laboratory via use of tissue culture. An immortalized cell line that retains important features of the conducting airway is 16HBE14o-. These cells

form tight junctions, maintain transepithelial resistance, and display vectorial ion transport (Cozens et al., 1994). Because the cells of the airways are one major target of inhaled particles and may be a significant site of absorption, this cell model was used to evaluate interactions between ENPs and the bronchial epithelium.

1.3.3 Skin structure and ENP exposure

Nanomaterials are present in wound dressings, drug delivery, cosmetics, detergents, food packaging, and other consumer goods. Topically applied ENPs are used in over 200 commercially available personal care products (Wiesenthal et al., 2011). Therefore, occupational and consumer settings also pose risk for ENP exposure through the skin. However, interactions between ENPs and human skin exposure remain largely unexplored (Crosera et al., 2009).

The skin is composed of three layers: the hypodermis which is composed primarily of adipose cells; the dermis, which provides structural support and is made up of connective tissue; and the epidermis, which is the outermost layer and performs the fundamental barrier function of the skin. This epithelial layer is multilayered, composed largely of keratinocytes, and is self-repairing and continually renewed. The basal layer of the stratified epithelium is composed of keratinocyte stem cells that divide to give rise to transient amplifying (TA) cells. These TA cells can differentiate as they move upwards in the epidermis. In this way, they move through the prickle cell layer, the granular layer and towards the

outermost layer of the skin, the stratum corneum, which is made up of keratinized cells that have lost their intracellular organelles (Figure 1.3) (Alberts et al., 2008).

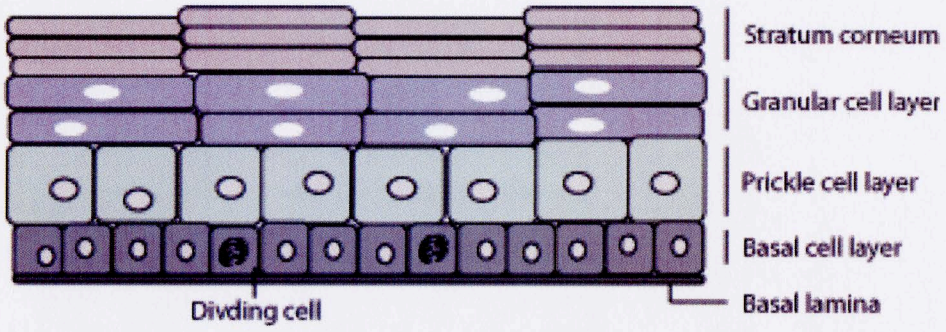

Figure 1.3: Layers of the epidermis. Cells divide in the basal layer, and move up through the layers above, changing their appearance as they move from one layer to the next.

Skin penetration has been shown for gold and silver nanoparticles in an *in vitro* system, with increased permeation in damaged skin (Larese et al., 2009; Larese Filon et al., 2011). Furthermore, these permeation studies with human skin showed that after a 24 hr exposure to silver nanoparticles, particles could be detected in the stratum corneum and the outermost surface of the epidermis by electron microscopy (Larese et al., 2009). Tissue culture is an effective method to study ENP effects on skin without the use of human skin samples or *in vivo* methods. HaCaT cells are immortalized human keratinocytes which respond to regulatory signals in a similar way to normal keratinocytes (Breitkreutz et al., 1998), and we therefore used the HaCaT cell line in this work to model how human skin interacts with ENPs.

1.4 Determinants of ENP toxicity

1.4.1 The effect of ENP size

The most obvious focus of ENP toxicity studies is on their size, which is in the range of typical cellular components and proteins, potentially allowing them to cross biological barriers and cause adverse or beneficial effects (Pan et al., 2007). Also, because ENPs occupy less volume than larger particles, they present a larger number of particles with a greater surface area per unit mass and increased potential for biological interaction (Oberdorster et al., 2005). Therefore, many studies have investigated the relationship between ENP size and toxicity.

One study examined the relationship between size and cytotoxicity of gold nanoparticles, which are used in biomedical imaging and diagnostic tests. Pan et al. exposed epithelial cell cultures to Au clusters between 0.8 to 15 nm. They found that HeLa cells (human epithelial carcinoma cell line) formed tight monolayers in the absence of the Au compounds, but those exposed to Au compounds showed membrane blebbing and vesicle formation at the plasma membrane following only one hour of exposure. After 12 hours, the cells were significantly swollen with fragmented nuclei, and many had lost both cell-to-cell and cell-to-substrate contact. Furthermore, particles 1-2 nm in size were highly toxic, whereas larger 15 nm particles were comparatively nontoxic, showing a clear relationship between size and toxicity (Pan et al., 2007).

However, there is not a consistent size-dependent cytotoxicity of ENPs among studies or even among ENPs. For example, a separate study showed three different sized SiO_2 nanoparticles had no difference in cytotoxicity (Cha and Myung, 2007). Additionally, there is considerable debate on the best dose metric for comparing different ENPs (Oberdorster, 2010). Both surface area and ENP number have been investigated; however, a more precise measurement for toxicity dose may be the biologically available surface area or surface reactivity (Oberdorster, 2010; Wittmaack, 2007). In order to approach this issue in our studies, calculated surface area concentrations (based on the measured mass concentrations exposed to cell cultures) were examined in relation to observed toxicity effects on 16HBE14o- cells.

1.4.2 Importance of ENP characterization

It is important to characterize the physicochemical properties of ENPs, such as size, distribution, shape, agglomeration, surface properties, solubility, and crystal structure, that may influence their toxicological activity (Oberdorster, 2010). A study on well-characterized metal oxide nanoparticles of similar nano-sizes instilled into lungs of rats showed varying inflammation responses to the ENPs. Of the ENPs tested that were inflammatory (CeO_2, NiO, ZnO, and CuO), each caused a different type of inflammation, indicating that the nano-size is but one of the characteristics that lead to inflammation (Cho et al., 2010). It is becoming increasingly clear that some combination of physical and chemical

features of individual ENPs is necessary to determine their intrinsic properties and biologic effects (Peralta-Videa et al., 2011).

A range of analytical techniques can be used to distinguish the structure and morphology for ENPs. Morphological characterization and size determination is commonly determined by transmission electron microscopy (TEM). Alternatively, the crystal structure can be obtained by powder X-ray diffraction (XRD) (Park et al., 2010). Spectroscopic related techniques are also used in ENP characterization. Dynamic light scattering (DLS) can be carried out in aqueous solution (as opposed to TEM which is performed in a vacuum) to determine the size distribution, aggregation condition, and electrophoretic mobility of ENPs (Peralta-Videa et al., 2011). DLS is employed to estimate the ENP dispersion through the attraction or repulsion between particles. Another measurement used to describe the aggregation of particles in solution is the zeta potential. A zeta potential is generated when charged particles are dispersed in a medium, and is a measure of the potential difference between the dispersion medium and the surface of the layer of fluid attached to the dispersed ENP. It can be related to the stability of the ENP dispersion, i.e. particles with a low zeta potential (negative or positive) tend to agglomerate, while those with a high zeta potential are stable dispersions (Thielbeer et al., 2011). Another mass spectrometry method, time-of-flight secondary-ion mass spectrometry (ToF-SIMS), is used to analyze surface chemistry, providing molecular information about the functional groups on the ENP surfaces (Baer et al., 2010).

1.4.3 Synthesis and life cycle of ENPs

Since the structure and form of an ENP is important to its function, there is an emphasis on the control of experimental conditions to produce uniform size, distribution, shape, chemical composition, and structure, and also to avoid agglomeration in the production of ENPs for most applications (Ju-Nam and Lead, 2008). There are many different methods to produce and control these parameters. ENPs can be generated directly from bulk materials with machining and etching methods like photolithography and laser-beam processing, or mechanical techniques like grinding and polishing. These techniques are termed "top-down" methods and deal with the reduction in structure sizes of microscopic elements to the nanometer scale in order to ultimately make electronic devices, computer chips, and microelectromechanical systems (MEMS) (Byrappa et al., 2008). Subsequent stabilization of the metal ENPs is usually obtained by adding colloidal protecting agents (Zhou et al., 2009). "Bottom-up" methods of synthesis control assembly of atomic and molecular aggregates into larger systems using chemical synthesis, self-assembly, and positional assembly (Byrappa et al., 2008). Stabilizers such as surfactants are necessary to control the initial growth of nanoclusters and to prevent agglomeration (Zhou et al., 2009). Typical products of these techniques are cosmetics, fuel additives, crystals, and displays (Byrappa et al., 2008). It is interesting to note that these distinct processes can introduce quite unique contaminants to the ENPs.

An active area of research is to refine nanoparticle processing methods to better synthesize ENPs with predictable and controllable properties. Chen and Gao used a novel and low-cost route to synthesize well-dispersed SnO_2 ENPs via a water-in-oil microemulsion-assisted hydrothermal process. In this process, the SnO_2 ENPs were created to specification for gas-sensing applications (typical of metal oxide semiconductors) from precursor inorganic tin salts (Chen and Gao, 2004). These refined synthesis methods are important for biomedical applications that usually require strictly controlled ENP size and morphology, e.g. in systems that control precisely the activity and drug delivery by the ENP. A secondary effect of changing synthesis methods is that ENP surface characteristics can be modified, which can impact the toxicity effects of ENPs.

No matter the processing method, ENPs can be released to the environment and exposed to humans. During ENP production and product manufacturing, workers can be directly exposed to ENPs through direct release or through the handling of dry powders. Workers involved in production of ENPs or ENP-containing products are at greater risks of exposure (inhalation and dermal) if powders are handled in non-enclosed systems, aerosols of ENPs are generated, ENP-containing materials are machined, sanded or drilled, or if maintenance and cleaning of production systems disrupts deposited ENPs. Exposure and environmental release can also occur during the life of the ENP-containing product, including use, recycling, and disposal. Human exposure to a wide variety of ENPs, either directly, or indirectly through the environment, is

possible in many ways. Although there is a lack of occupational exposure measurements and environmental ENP concentrations, it is important to study the toxicology of these newly produced particles. The variety of applications of ENPs provides many opportunities for human exposure, including during manufacturing processes, disposal of wastes, and use of the products.

1.5 *In Vitro* Models of ENP exposure

Since the applications of ENPs are rapidly growing, more and more ENPs are being produced, and humans are increasingly exposed to ENPs in both occupational and medicinal situations. With this increased exposure, it becomes necessary to carefully assess the toxicology of these emerging ENPs, as well as their interactions with biological systems. The EPA has recognized the risk of nanomaterials to human health and has established an international collaborative project engaged in identifying alternative test methods for nanotoxicology. This effort is focused on establishing *in vitro* and other alternative methods for reduction, refinement, or replacement of animals in tests (EPA, 2011). Although *in vitro* systems are limited to one cell type (or a combination of a few) and therefore may not properly replicate interactions between a variety of cell types, they are easy to use, control, and interpret for cytotoxicity studies. With the quickly increasing numbers of potentially toxic ENPs that need to be tested, *in vitro* models are essential to assess the hazards of these materials (Stone et al., 2009).

1.5.1 Toxicity Testing Methods

There are a variety of *in vitro* assays used to obtain toxicity data. This section is not meant to be an exhaustive resource, rather an introduction to some of the most commonly used *in vitro* toxicity assays, including those utilized in this thesis. Additionally, it is thought that the discussed assays best reflect the ability of ENPs to induce toxic effects on humans.

A common *in vitro* assay is based on 3-(4,5-Dimethylthiazol-2-yl)-2,5-diphenyltetrazolium bromide (MTT) color changes. MTT is a tetrazolium salt that reduces to formazan in metabolically active (i.e. healthy) cells. In the mitochondria, dehydrogenases cleave the tetrazolium ring, yielding purple MTT formazan crystals, which are dissolved with detergent. The purple product can then be quantified by light absorbance. Based on cell type-specific relationships that associate an increased absorbance to an increase in cell number, cell number and viability can be determined to detect changes in proliferation and cytotoxicity.

Another common, non-fluorescent system used to evaluate toxicity to cells is the lactate dehydrogenase (LDH) assay based on membrane damage of dead cells. LDH is a stable enzyme found in the cytoplasm of all cell types, but is released into the cell culture medium upon damage to the plasma membrane, an indicator of a reduction in cell viability. Assays that detect increased LDH in the extracellular fluid are indicative of a decrease in cell viability.

Fluorescent-based cell viability assessment can also be used to simultaneously determine live and dead cells after exposure to ENPs. One of the most common microscopy-based fluorescent assays is the "Live/Dead" assay (Invitrogen). This assay utilizes the membrane-permeant calcein-acetomethoxy ester (calcein-AM), which is cleaved by non-specific esterase activity in live cells, yielding a cytoplasmically trapped green fluorescence (ex/em ~495 nm/~515 nm) dye (calcien). Calcein detection of live cells is coupled with the charged and membrane impermeant ethidium homodimer-1 (EthD-1). This dye can enter membrane-compromised cells (i.e. dead cells) and interact with nucleic acids to display a "red" fluorescence (ex/em ~495 nm/~635 nm). Upon excitation with 495 nm light, live cells (i.e., ones with intact plasma membranes and active esterases) appear green and dead cells (i.e., ones with compromised plasma membranes that allow for passage of EthD-1) appear red. The ratio of green to red cells within a population can be used as a quantitative measure of cytotoxicity.

A disadvantage of fluorescence-based assays is that there is a potential for fluorescence interference with the ENPs and assays require analysis at individual time points. However, cell-based label-free technologies are available to assess cytotoxic responses over time. By avoiding the use of fluorescent dyes, these assays allow the cells to grow and act in their native environment without any potential negative effects of a label that could influence cellular processes. Furthermore, they produce real-time kinetic measurements by

monitoring the cells for the entire span of the experiment, instead of just a snapshot of the chosen endpoint. Therefore, in addition to the fluorescent Live/Dead assay, we utilized the Roche xCELLigence real time cell analyzer (RTCA) system to examine the cytotoxicity of ENPs to cell cultures. The RTCA system is based on electronic detection of biological assay processes. Microelectronic cell sensor arrays, which measure the electronic impedance, are integrated into the bottom of 96-well plates (E-plate). The RTCA system measures the electronic impedance of the sensor electrodes, allowing changes in cells on the electrodes to be detected and monitored. Cell viability, cell number, cell morphology, and degree of adhesion can affect electrode impedance. Relative changes in electrical impedance are expressed by the dimensionless "cell index" parameter, which is derived by dividing the impedance change by a background value. When cells are introduced into the wells of the E-plate, they make contact with and attach to the sensor electrode surfaces. The sensors are monitored with the RTCA Station, which may be placed inside a tissue culture incubator to allow for normal cell growth conditions. With the RTCA system, cell index can be monitored during cell growth and experiments to provide quantitative information about the biological status of the cells. We developed optimal conditions for RTCA experiments that test ENP cytotoxicity to both of our cell models (HaCaT and 16HBE14o-), as well as for experiments that examine cell-signaling responses of 16HBE14o- cells.

1.5.2 ENP Dosimetry

There is significant discussion and lack of agreement on the best method for ENP dosimetry in toxicity studies: mass, number, and surface area measures have all been used to describe exposure, or administered ENP doses to cells. Not only are exposure doses inconsistently represented among studies, but they also have failed to produce *in vitro* systems that can predict an *in vivo* response, possibly because these exposure doses are not reliable measures of target cell dose across particle size or systems (Teeguarden et al., 2007). Exploring the relationship between dosimetry and toxicity or biological responses is important both to scale data across studies and to evaluate how the intrinsic surface chemistry of the material changes as the material approaches the nanoscale.

Since ENPs settle, diffuse, and agglomerate, they do not act the same as soluble chemicals. Therefore, we cannot assume that the same administered ENP dose will give consistent cellular doses in *in vitro* systems across particle types with varying size, density, and physicochemical properties. Settling and diffusion rates of ENPs dependent on particle properties could greatly affect transport rates to the cell (Figure 1.4), and consequently affect relative toxicity (Hinderliter et al., 2010). A better measure would be a more direct cellular dose, but this is often difficult to quantify experimentally. Instead, Hinderliter et al. proposed a computational model that accounts for the dynamics of particles in liquids to describe the influence of diffusion and gravitational settling on particle

transport to cells *in vitro* (Hinderliter et al., 2010). The I*n vitro* Sedimentation, Diffusion and Dosimetry model (ISDD) is based on the principles of Stokes sedimentation and Stokes-Einstein diffusion and calculates, based on inputs that are easily available (temperature, media density and viscosity, media height, hydrodynamic particle size, and particle density), a delivered dose to the cell. This cellular dose is a measure of particles associated with the cell, either on or in the cell. The ISDD model can also account for agglomeration of ENPs by incorporating agglomerate sedimentation velocity.

Using a method like ISDD to consider system kinetics and obtain a more accurate measure of the ENP dose delivered to the target tissue will better allow particle types and doses to be compared among studies. In the current work, we used this model to examine the time course in which the tested ENPs are delivered to the cell cultures, demonstrating that parameters such as media height and particle size affect the fraction of administered dose that is deposited onto the cells. When comparing cytotoxicity of particles across studies, it is important to consider these diffusion and sedimentation determinants with respect to dosimetry.

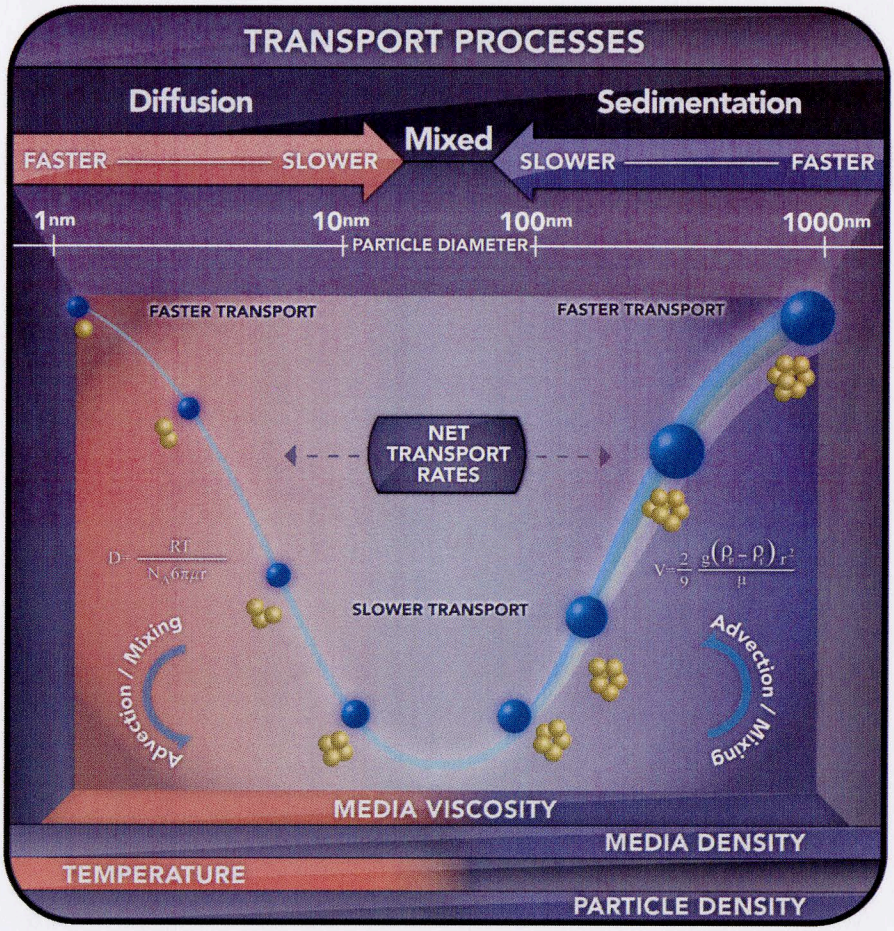

Figure 1.4: Transport rates of nanoparticles *in vitro* are affected by transport processes such as diffusion and sedimentation. Transport is controlled mostly by diffusion for particles ≤ ~10 nm and is controlled by sedimentation for particles greater than ~200 nm. Transport is fast when one mechanism dominates, but becomes slower when neither diffusion nor sedimentation is particularly effective (particles sizes between 10 and 100 nm). Reprinted with permission (Creative Commons Attribution License) (Hinderliter et al., 2010).

1.5.3 Nanoparticle interactions with the dispersion medium

The physicochemical properties of the ENPs contribute to the dynamic interactions between the ENP surface and the biological medium, including

formation of a protein corona (Figure 1.5). When ENPs enter a biological fluid, or in the case of *in vitro* studies, a dispersion medium, their composition can be affected by the proteins of the medium that come in contact with the ENP surface. Proteins that coat the ENP make up the protein corona and they influence the ENP surface properties, charge, aggregation tendencies, and hydrodynamic size. The protein corona is associated with how the ENPs interact with cell membranes and receptors (Nel et al., 2009). These interactions can influence the cytotoxicity of an ENP and potentially lead to either more biocompatible or more bioadverse outcomes. This is particularly important to consider for *in vitro* assays, since the interaction of ENPs with serum in the suspension media can significantly affect their resultant toxicity *in vitro* (Clift et al., 2010). Therefore, ENP properties should be assessed in the dispersion medium used for *in vitro* experiments, since properties like hydrodynamic size can change once suspended in the medium. In our studies, we examined the size of HfO_2 ENPs in different mediums, and found that the particle size distribution of this metal oxide ENP varies significantly depending on suspension medium. Thus, the exposure medium likely contributes to observed cytotoxicity.

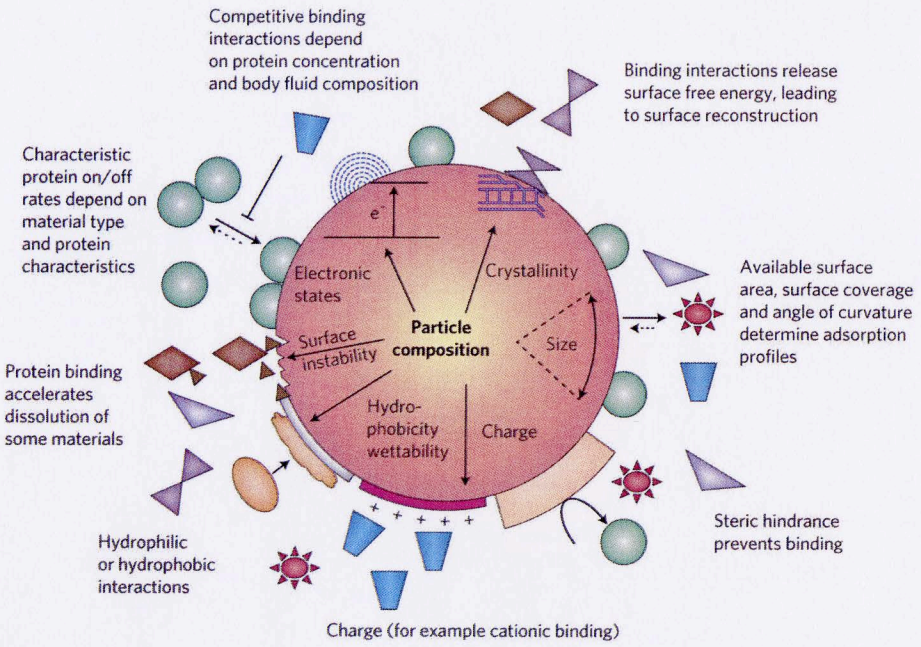

Figure 1.5: The protein corona surrounding an ENP can influence cytotoxicity effects. ENP characteristics determine the formation of the corona in the biological environment. Reprinted by permission from Macmillan Publishers Ltd: Nature Materials, (Nel et al., 2009), copyright 2009.

1.5.4 The effect of ENP exposure on cell signaling

Although it is important to determine the toxicity parameters of newly developed ENPs, it is also necessary to investigate the cellular and molecular mechanisms that lead to this toxicity. Previous research into air pollution, mineral dust particles, and diesel exhaust particles (DEP) provides a starting point for potential mechanisms of toxicity that lead to lung injury. For instance, ultrafine particles in air pollution (<100 nm) have been shown to cause oxidative stress and pro-inflammatory effects, both in *in vivo* and *in vitro* models, as well as

changes in intracellular Ca^{2+} signaling (Baulig et al., 2003; Donaldson and Stone, 2003). Similar reactions have been shown for ENP exposure. For example, cultured cells exposed to cerium oxide and silica nanoparticles show an increase in reactive oxygen species (ROS), a decrease in the antioxidant glutathione (GSH), as well as other signs of oxidative stress (Akhtar et al., 2010; Park et al., 2008).

A three-tiered stress model has been proposed to explain cellular responses to increasing levels of stress caused by ENPs (Xia et al., 2008). In the Tier 1 level, low levels of stress produce protective cellular responses, e.g. anitoxidant enzymes induced to combat ROS. Tier 2 stress levels, however, can cause damaging effects that do not yet cause cell death, including alterations in cell signaling, innate immune responses, and transcription. The third tier of the model involves stress levels that cause cell death, either by apoptosis or necrosis.

Many ENP toxicity studies demonstrate dose-dependent effects using cellular models, but most of these use exposure concentrations that are much greater than realistic human exposure scenarios. These high concentrations likely approach Tier 3 of the stress model in order to cause cytotoxicity. However, even if low ENP exposure levels do not kill cells, this does not mean that the cells are not affected. For example, A549 human alveolar cells cultured with alveolar macrophages exposed to benign concentrations of aluminum ENPs showed impaired phagocytic function and altered immune response activation.

This demonstrated that although the ENPs were not toxic to the cells, they did impair the cell's innate ability to respond to a respiratory pathogen (Braydich-Stolle et al., 2010). These affects fall under the Tier 2 level of stress outlined by the hierarchal stress model (Xia et al., 2008).

Autocrine/paracrine purinergic (ATP) signaling is an important part of cellular coordination in the airway epithelium. For example, purinergic signaling in the airway epithelium can mediate responses to bacteria and oxidative stress (Ahmad et al., 2006; Boots et al., 2009), and alterations in airway ATP signaling have been linked to chronic lung diseases like COPD (Lommatzsch et al., 2010). Coordinated Ca^{2+} signaling, mediated by ATP, is also important in lung defense strategies, e.g. ATP signaling can regulate intracellular Ca^{2+} concentration ($[Ca^{2+}]_i$) to increase ciliary beat frequency (Lieb et al., 2002).

The intracellular messenger Ca^{2+} is extremely versatile and universal, and is involved in diverse cellular regulation in almost all cell types throughout their lifetime. The Ca^{2+} ion precisely regulates multiple functions, including triggering fertilization, controlling development and differentiation, and diverse cellular functions. Ca^{2+} signaling outcomes depend on increased levels of $[Ca^{2+}]_i$ that can originate from outside the cell or from sources inside the cell, including the endoplasmic reticulum stores. Duration, location, and amplitude are all parameters of the Ca^{2+} signals that affect the coordination of complex physiological processes (Berridge et al., 1998).

Any disturbance in these Ca^{2+} signals can modify the physiological outcome to affect normal cell functions. Oxidative stress has been shown to impact Ca^{2+} signaling, and has been examined in relation to nanoparticle exposure and cell viability. Human lung epithelial cells (BEAS-2B) exposed to ZnO ENPs demonstrated cytotoxicity, while showing elevated oxidative stress and increased $[Ca^{2+}]_i$ levels in a time- and concentration-dependent manner. The elevation in $[Ca^{2+}]_i$ was partially attenuated by the antioxidant N-acetylcysteine (NAC), linking oxidative stress to disrupted Ca^{2+} homeostasis (Huang et al., 2010). These $[Ca^{2+}]_i$ disruptions are seen even at non-cytototoxic concentrations of ZnO nanoparticles (Wang et al., 2010). These studies indicate that the cellular response to ENPs alter Ca^{2+} signaling.

We hypothesized that ENP exposure to the airway epithelium could compromise innate immunity functions even at benign ENP levels. Therefore, in the present study, human bronchial epithelial cells were exposed to non-cytotoxic concentrations of ENPs, and their response to extracellular ATP was investigated. Indeed, these benign concentrations of ENPs caused reductions in cellular responses to ATP and reductions in Ca^{2+} signaling in response to ATP.

1.6 Summary

From the limited ENP studies available, it is evident that many ENPs cause negative health effects, including lung and airway-specific compromise following inhalation of the particles. Despite the rapidly increasing number of

ENPs being produced and exposed to humans and the environment, coordinated toxicity assessments are not currently in effect. *In vitro* techniques that model *in vivo* events are imperative to test the toxicity of new ENPs and to better understand their mechanisms of action. In the present study, cell cultures were used to assess metal oxide ENP toxicity to skin and lung epithelium. A real time cell analysis (RTCA) cytotoxicity assay was developed to build upon the toxicity data collected from an endpoint Live/Dead assay. Where minimal ENP toxicity was seen, it was hypothesized that cellular functions of innate immunity are disrupted by ENP exposure despite a lack of cell death. Therefore, the effect of ENP exposure on purinergic signaling was investigated. RTCA and intracellular calcium imaging were used to test the effect of ENP exposure to lung epithelium on the cellular response to ATP.

CHAPTER 2 - MATERIALS AND METHODS

2.1 Materials

Minimum essential medium with Earle's salts (MEM), Dulbecco's modified Eagle's medium (DMEM), Lechner and LaVeck (LHC) basal medium, Hanks' balanced saline solution (HBSS), penicillin, and streptomycin were purchased from InVitrogen Corporation (Carlsbad, CA). Fibronectin and type I collagen were purchased from Becton-Dickinson (Franklin Lakes, NJ). GlutaMax, fetal bovine serum (FBS), and ATP were purchased from Sigma-Aldrich (St. Louis, MO). E-plates were purchased from Roche Applied Sciences (Indianapolis, IN). Fura 2-acetoxymethyl ester (fura 2-AM) and fura-2 were purchased from Calbiochem (La Jolla, CA).

2.2 Nanoparticle sources

All batches of HfO_2 were obtained as dry powders. HfO_2 batch 1 (manufacturer reported size of 20 nm) and HfO_2 batch 2 (manufacturer reported size of 2 nm) were a gift from Cornell University, Dept of Material Science and Engineering, Ithaca NY, USA. Batch 2 contained 10% wt/wt acetic acid. HfO_2 batch 3 (manufacturer reported size of 100 nm) of 99.9% purity was acquired from American Elements Co, Los Angeles, CA, USA. A reference micron size HfO_2 (manufacturer reported size of <44 μm) of 99.95% purity was obtained from Alfa Aesar Co, Ward Hill, MA, USA. CeO_2 (manufacturer reported size of 50 nm,

99.95% purity) and SiO_2 (manufacturer reported size 10-20 nm, 99.5% purity) nanoparticles were obtained from Sigma Aldrich (St. Louis, MO, USA). Reference micron size SiO_2 (manufacturer reported size <5 μm, 99.995% purity) and micron size CeO_2 (powder, 99.9% purity) were also obtained from Sigma Aldrich.

2.3 Particle size distribution (PSD) and zeta potential measurements

PSD and zeta potential measurements were made in the laboratories of Drs. Reyes Sierra-Alvarez and Jim Field, University of Arizona by Antonia Luna and Lila Otero Gonzalez. The zeta potential of ENPs dispersions was measured with a Zeta Sizer Nano ZS (Malvern, Inc., Sirouthborough, MA) using laser doppler velocimetry (LDV). This technique uses a laser, which is passed through the sample, to measure the velocity of the particles in an applied electric field of a known value (electrophoretic mobility). The instrument uses the Smoluchowski equation to correlate particle electrophoretic mobility to zeta potential. PSD measurements were determined by dynamic light scattering (DLS) using the same instrument. The unit employs a 4mW He-Ne laser (633 nm) and a measurement angle of 173°. The refractive indices used for CeO_2, SiO_2, Al_2O_3, and HfO_2 were 1.828, 1.487, 1.765, and 1.990, respectively. Laser diffraction was performed by an outside lab to determine PSD measurements for micron-sized HfO_2 and SiO_2. Particles were analyzed in a water dispersion using a Mastersizer Hdyro 2000S (Malvern Instruments, Ltd.).

2.4 Transmission electron microscopy

Transmission electron microscopy (TEM) was performed by Antonia Luna, University of Arizona. ENP samples were examined by TEM to gain information on particle morphology and size. A Hitachi H8100 TEM instrument was used at 200 keV. Its point-to-point resolution is 2 Å for the high-resolution pole piece and 2.3 Å for the analytical pole piece.

2.5 Cell culture

The HaCaT human kerotinocyte skin cell line was a kind gift from Dr. Anne Cress (Dept. Cell Biology and Anatomy, University of Arizona). Cells were grown in full growth medium that consisted of DMEM supplemented with 10% (v/v) FBS, penicillin, and streptomycin at 37°C in a 5% CO_2 atmosphere. Growth medium was replaced every other day until the cells reached confluence. Cells were expanded in flasks prior to passage onto 24-well plates for Live/Dead studies or 96-well E-plates (Roche Applied Sciences) for assays using the xCELLigence real time cell analyzer (RTCA; Roche Applied Sciences).

16HBE14o- cells are a SV40 transformed human bronchial epithelial cell line (Gruenert et al., 1995) and were obtained through the California Pacific Medical Center Research Institute (San Francisco, CA). 16HBE14o- cells were grown on a collagen/fibronectin bovine serum albumin (BSA) matrix (CFB; 88% LHC basal medium, 10% BSA, 1% bovine collagen type I, and 1% human fibronectin) in a full growth medium that consisted of MEM supplemented with

10% (v/v) FBS and 2 mM glutamax, penicillin, and streptomycin at 37^0C in a 5% CO_2 atmosphere. Growth medium was replaced every other day until the cells reached confluence. Cells were expanded in flasks prior to passage onto 24-well plates for Live/Dead assays, 96-well E-plates for RTCA studies, or onto 15 mm glass coverslips for microscopy studies.

2.6 Live/Dead assay

HaCaT cells were plated onto a 24-well plate at a density of 4,000 cells/cm^2 in full growth medium. The medium was replaced every third day until the cells reached confluence (4-7 d). Just prior to experimentation, the stock solution of ENPs was briefly sonicated, vortexed, and then diluted with HBSS (1.3 mM $CaCl_2$, 5.0 mM KCl, 0.3 mM KH_2PO_4, 0.5 mM $MgCl_2$, 0.4 mM $MgSO_4$, 137.9 mM NaCl, 0.3 mM Na_2PO_4 and 1% glucose additionally buffered with 25 mM HEPES, pH 7.4) to establish working concentrations. Cells were washed twice with HBSS to remove medium, and exposed to the appropriate concentration of HfO_2 for 2 h at 37°C. Cells were then washed twice with HBSS, and subjected to the Live/Dead assay as per manufacturer's protocol (Invitrogen). Wells were examined on an Olympus IX70 microscope using epifluorescence and a dual-color cube. Six pre-determined areas from each well were captured, using a CoolSnap color camera (Roper Scientific, Tucson, AZ), and displayed on a Macintosh G4 computer. Total cells, live cells (green) and dead cells (red), were counted for each frame by a blinded observer and the percentage of live cells

representing each well were determined. A minimum of four wells were measured at each ENP concentration during each experiment. Live/Dead assays on 16HBE14o- cells were handled similarly, excepting that cells were plated in full growth medium at a density of 110,000 cells/cm^2 onto 24-well plates coated with CFB.

2.7 Cytotoxicity assay with Real Time Cell Analyzer (RTCA)

16HBE14o- cells were plated in full growth medium at a density of 100,000 cells/well (510,000 cells/cm^2) onto 96-well E-plates (Roche Applied Science) coated with CFB solution. The cells were allowed to grow at 37°C in a 5% CO_2 atmosphere while relative impedance of each well was monitored in 15 min intervals using the RTCA device (Roche Applied Science). The RTCA measures relative impedance changes over time at the surface of each well to determine physiological changes in adherent cells that can be related to proliferation, cytotoxicity, or cellular signaling (Abassi et al., 2009). Relative impedance at any given time is expressed as "cell index." Cell index is defined as $(Z_i - Z_o)/(15\Omega)$, where Z_i is impedance at a given time point during the experiment and Z_o is impedance before the addition of the ENP. Average cell index for each ENP dose ($n \geq 4$) was graphed over time. The E-plate was removed from the RTCA and ENPs were added to the cell cultures when the average cell index reached a value corresponding to ~80% confluence, where 100% confluence is the cell index at which a plateau is reached. Cells were washed twice with serum-free

growth medium, and exposed to appropriate concentrations of the ENP being tested, then returned to RTCA at 37°C and 5% CO_2. For continued cell index monitoring. RTCA cytotoxicity assays on HaCaT cells were handled similarly, except that cells were plated in full growth medium at a density of 15,000 cells/well (76,400 cells/cm^2) onto E-plates coated with poly-L-lysine.

2.8 ATP Dose Response Curves Using RTCA

16HBE14o- cells were plated onto a 96-well E-plate (Roche Applied Science) as indicated for the RTCA cytotoxicity assay, with cell index monitored in 15 min intervals overnight at 37°C and 5% CO_2 by RTCA. At a cell index indicating ~40% confluence, full growth medium was replaced with full growth medium or full growth medium supplemented with the ENPs being tested, and the E-plate was returned to the RTCA at 37°C and 5% CO_2 for continued 15 min interval monitoring of cell index. After 24 hr, the E-plate was removed from the RTCA, brought to room temperature, and then the cells were washed with HBSS with the appropriate ENP concentration. Increasing concentrations of ATP (100 nM to 100 μM in ½ log steps, supplemented with the appropriate ENP concentration) were administered to the E-plate wells from previously prepared transfer plate wells. The E-plate was returned to the RTCA at room temperature immediately after ATP addition. Cell index was recorded in 15 sec intervals for 4 hrs. Cell responses were collected from at least 4 wells and adjusted to a baseline by ratioing with recordings from cells washed with HBSS alone. Total

integrated cellular responses were calculated from the area under the curve for each ATP dose (Sherwood et al., 2011).

2.9 Intracellular Ca^{2+} Concentration ($[Ca^{2+}]_i$) Measurements and ATP wash experiments

16HBE14o- cells were plated in full growth medium (as previously described) at a density of 200,000 cells/well (110,000 cells/cm^2) onto 15 mm glass coverslips. The medium was replaced every third day until the cells reached confluence (4-6 d). 24 hrs prior to experimentation, the medium was replaced with full growth medium or full growth medium supplemented with the ENPs being tested. Prior to imaging, 16HBE14o- monolayer cultures were washed with HBSS or HBSS supplemented with ENPs and then loaded for 40 min in 5 μM fura 2-AM loading solution or fura-2AM loading solution supplemented with the appropriate concentration of ENP. Coverslips were returned to the appropriate HBSS solution for at least 20 min before Ca^{2+} imaging. Fura-2 fluorescence was observed on an Olympus IX70 microscope with a 40X oil immersion objective after alternating excitation between 340 and 380 nm by a 75 W Xenon lamp linked to a Delta Ram V illuminator (PTI, London, Ontario) and a gel optic line. Images of emitted fluorescence above 505 nm were recorded by an ICCD camera (PTI) and simultaneously displayed on a 21" Vivitron color monitor. The imaging system was under software control (ImageMaster, PTI) and collected a ratio approximately every 0.6 sec. $[Ca^{2+}]_i$

was calculated by ratiometric analysis of fura-2 fluorescence using equations originally published in (Grynkiewicz et al., 1985). A typical experiment consisted of 20 sec of recording of cells in HBSS or ENP-supplemented HBSS to determine resting $[Ca^{2+}]_i$, followed by a ~10 s wash to apply ATP solution. Cells were monitored for an additional 160 sec. A change in $[Ca^{2+}]_i$ was considered positive if the cell increased $[Ca^{2+}]_i$ to 200 nM or more.

2.10 Statistics

Data were compared using a one-way ANOVA with Tukey's Multiple Comparison Test, unless otherwise noted. A value of $P < 0.05$ was used to establish significant difference between samples. Figures are graphed ± standard error of the mean (SEM).

CHAPTER 3 - RESULTS

3.1 Characterization of HfO_2 ENPs demonstrates differences between manufacturer

Differences in size and physicochemical properties of nanoparticles may affect their toxicity. To investigate how size affects toxicity, four batches of the same type of ENP, HfO_2, from different sources were evaluated for average particle size, size distribution, zeta potential, and surface chemistry prior to examining the cytotoxicity of each batch. Previous studies have shown smaller particle size corresponds to increased surface area and therefore greater biological effects. Therefore, we hypothesized that smaller HfO_2 ENPs would cause the highest levels of cytotoxicity. These characterization studies were carried out as part of a Semiconductor Research Corporation collaboration between Drs. Reyes Sierra-Alvarez, Jim Field, Farhang Shadman, and Scott Boitano, from the University of Arizona, and Dr. Buddy Ratner from the University of Washington (Field et al., 2011).

The stated primary size of HfO_2 batches 1, 2, and 3 were 20 nm, 2 nm, 100 nm, respectively, and the micron HfO_2 particles were reported to be <44 μm in size. (Figure 3.1, Table 1). Measurements to verify the sizes showed that the size reported by the supplier did not agree with the measured size for any of the batches. The measured particle size distribution (PSD) of samples 1-3 are shown in Figure 3.2, and the PSD of the micron batch is shown in Figure 3.3.

The average hydrodynamic particle size of HfO_2 ENPs dispersed in pH 4 dilute acetic acid was measured by dynamic light scattering (DLS) and ranged from 150 to 286 nm for the nano-sized particles (Figure 3.2). Batch 3 samples had the lowest average size of 150 nm, but the PSD shows that a portion of the particles spans the nano-region (<100 nm) and were therefore considered "nanoparticles" in this study. The PSD of the micron HfO_2 was measured with laser diffraction and had an average particle size of 6.768 µm, which agrees with the supplier-reported size of <44 µm (Figure 3.3). Particle size measurements were also made with TEM and SEM images, but only batch 3 and micron HfO_2 samples produced measurements with good correspondence between the DLS measurement. Agglomeration and crystal formation were visible in TEM images of batches 1 and 2 (Figure 3.1).

Table 1: Particle size characterization of the different samples of HfO_2 ENPs. ENPs were suspended in 100 mg L^{-1} solution of acetic acid adjusted to pH 4, followed by ultrasonic treatment (130 W, 20 KHz, 60% amplitude) for 5 min and particle size was measured with dynamic light scattering (DLS), performed by Antonia Luna, University of Arizona.

Parameter	Batch 1	Batch 2	Batch 3	Micron
Size reported by supplier (nm)	20	2	100	<44,000
DLS/Diffraction (nm)	286	283	150	6,768[#]
TEM/SEM images diameter (nm)	1000-5000[*]	2000-8000[**]	150-260	300-1000
Zeta potential (mV)[+]	52	44	66	64

[#]PSD measured by laser diffraction in water dispersion using Mastersizer Hydro 2000S Malvern (Sasol Italy R&D)
[*]visible as agglomerates
[**]crystalline formation visible

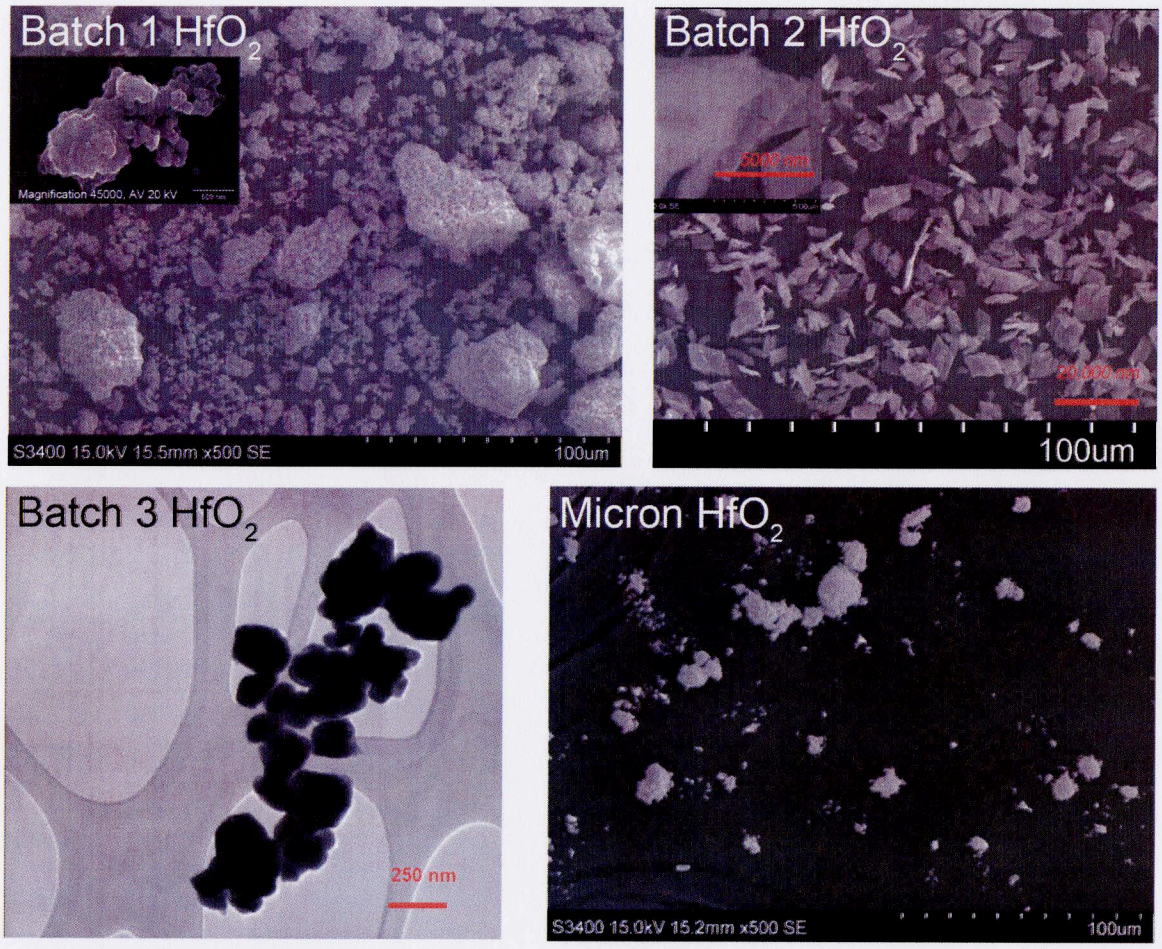

Figure 3.1: TEM images of each HfO_2 batch used in this study. Particles of different batches varied in size and shape and displayed particle agglomeration. Average particles sizes did not agree with the sizes reported by the supplier (Table 1). Images were provided by Antonia Luna, University of Arizona.

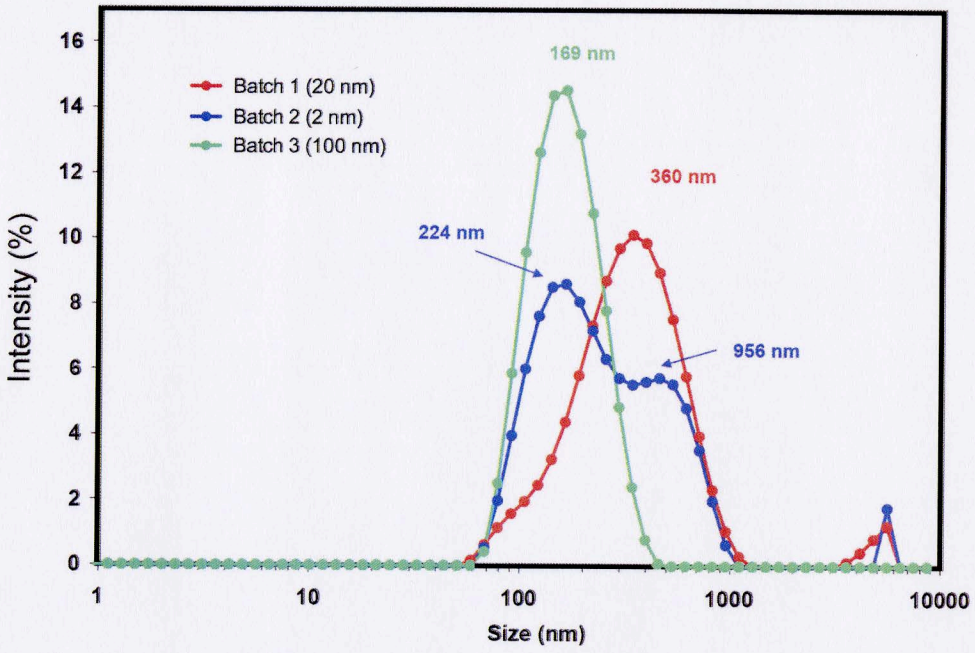

Figure 3.2: Particle size distribution of HfO_2 ENP batches 1-3. Particle size distribution of the different batches of HfO_2 ENPs based on light intensity. The sizes noted on inset legend refer to the manufacturer reported size. Samples were prepared in pH 4 in 100 mg L^{-1} acetic acid. Average diameters for each batch are shown in Table 1. Measurements were performed by Antonia Luna, University of Arizona.

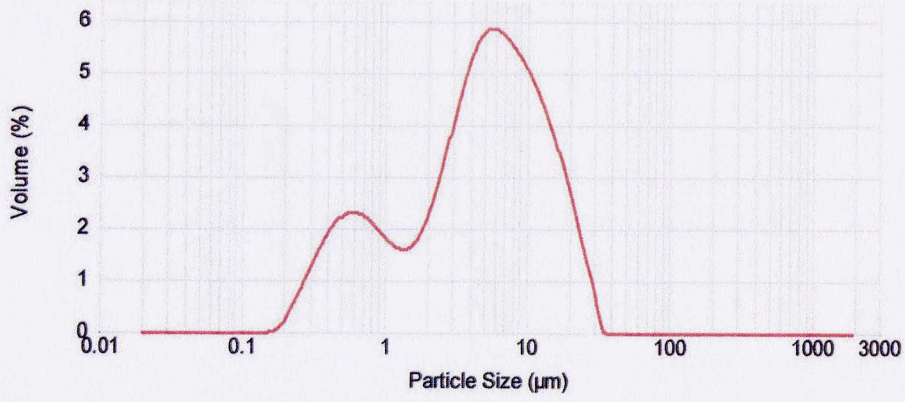

Figure 3.3: PSD for HfO_2 micron batch. PSD for the HfO_2 micron batch was analyzed with laser diffraction in a water dispersion with a Mastersizer Hydro 2000S Malvern (Sasol Italy R&D). Although the stated particle size was <44 µm, the measured volume weighted mean was 6.768 µm.

Since the medium used to suspend and administer the ENPs to the *in vitro* culture can potentially affect the PSD, ENPs of one HfO_2 batch were dispersed in various media, and the PSD was measured for each dispersion. Batch 3 was the focus of further experiments in this study, and was therefore chosen for this comparison. PSD of batch 3 HfO_2 ENPs was measured in Milli-Q water (ultrapure, deionized; Millipore), Milli-Q water with polyacrylate dispersant (Dispex), MTT medium (DMEM supplemented with 5% FBS), or HBSS at pH 7.2 (Figure 3.4). Compared to the PSD in dilute acetic acid, the PSD of batch 3 HfO_2 was larger in Milli-Q water with an average 359 nm, indicating that the neutral pH causes agglomeration and a shift to larger average particle size. The addition of Dispex (a polyacrylate dispersant) to Milli-Q water reduced the PSD by reducing the interaction between the HfO_2 ENPs. MTT medium also caused a decrease in PSD compared to Milli-Q water. HBSS, a balanced salt solution, as a dispersion medium greatly increased PSD, producing an average particle size of 3.242 µm. This increase may be due to the salts increasing the tendency of the NPs to agglomerate. The variation in agglomeration among suspension mediums emphasizes the importance of characterizing the size of particles in the medium that is applied to cell cultures for *in vitro* experiments.

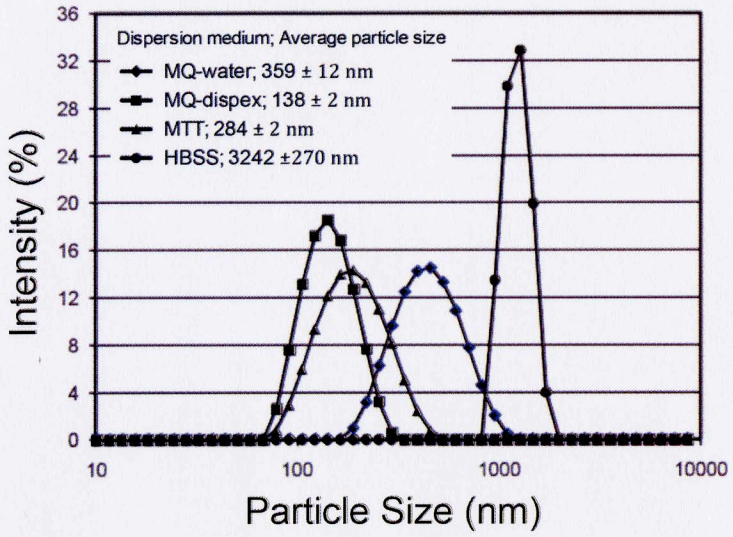

Figure 3.4: Particle size distribution of batch 3 HfO_2 ENPs in different media (MQ-water, MQ-dispex, MTT, or HBSS) at pH 7.2. The dispersion medium can affect particle size. Particles in HBSS had the largest average particles size of 3,242 nm. Average particle size for each media is displayed in the legend. Measurements performed by Antonia Luna, University of Arizona.

3.2 Characterization of SiO_2 and CeO_2 ENPs

In addition to comparing ENP size characteristics between batches of HfO_2 ENPs, silicon oxide (SiO_2) and cerium oxide (CeO_2) ENPs were examined. TEM images were used to visualize the particles (Figure 3.5) and DLS was used to determine the size distribution in aqueous solutions (Figure 3.6). CeO_2 (reported size, 50 nm) had an actual average size of 132 nm, and SiO_2 (reported size, 10-20 nm) was 368 nm, as measured by DLS (Table 2). Similar to the findings with HfO_2 ENPs, the SiO_2 and CeO_2 reported sizes did not agree with the average measured size.

An important lesson is highlighted here, that data provided by the particle supplier should be reconfirmed prior to assessing their toxicity properties. Also, wet phase (DLS) measurements are likely reflective of agglomeration in the solvents. In future experiments, it would be imperative to accurately assess the sizes of the particles delivered to the cells in order to gain reliable relationships between particle size and effects on cells.

Table 2: Particle size characterization of SiO_2 and CeO_2 ENPs.

Parameter	Nano-SiO_2	Nano-CeO_2	Micron-SiO_2	Micron-CeO_2
Size reported by supplier	10-20 nm	50 nm	powder	< 5µm
DLS/diffraction average diameter (nm)[+]	368 ± 3	132 ± 1	212,800	ND
Zeta potential (mV)	-39.2 ± 0.3	44.5 ± 1.1	ND	ND
pH[*]	7.32	3.40	ND	ND

ND indicates not determined
[*]pH value of the dispersion tested for particle size distribution

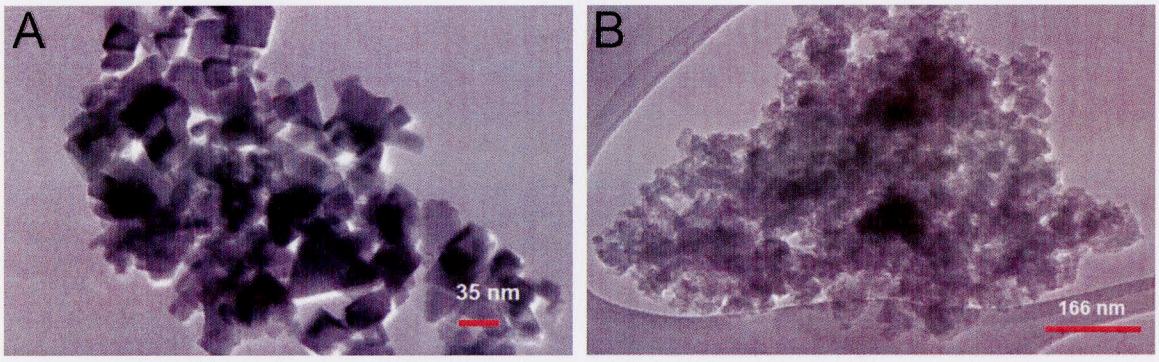

Figure 3.5: TEM images of (A) CeO_2 and (B) SiO_2 used in this study. CeO_2 ENPs were cube-shaped and SiO_2 were more typically spherical. Agglomeration appeared to be a potential problem. Images were taken by Lila Otero Gonzalez, University of Arizona.

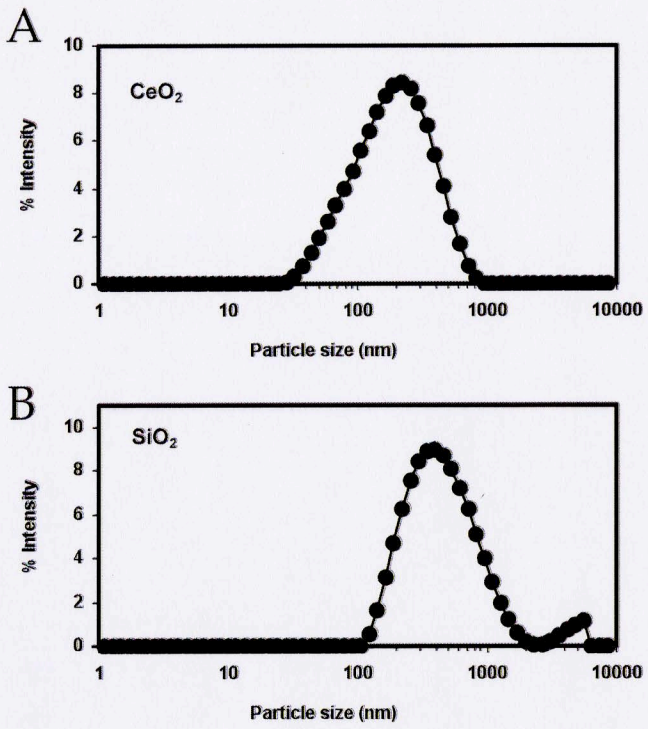

Figure 3.6: Particle size distribution of (A) CeO_2 and (B) SiO_2 ENPs in aqueous solutions with pH values of 7.50 and 7.32, respectively. The size distributions span an entire log, showing large variation in particle size. Average particle sizes are listed in Table 2. Measurements were done by Lila Otero Gonzalez, University of Arizona.

3.3 ENP cytotoxicity evaluations

Multiple assays were used to evaluate the cytotoxicity of ENPs. The fluorescent Live/Dead assay was used to investigate effects of select ENPs at single time points (2 hrs after exposure), and, once developed, the non-fluorescent RTCA assay was used to examine ENP effects over time.

3.3.1 Cytotoxicity comparison between HfO_2 from different suppliers with Live/Dead assay

In order to relate the size characterizations of the four HfO_2 particle batches to cytotoxicity, Live/Dead assays were performed on each batch. HaCaT cell cultures were exposed to the HfO_2 ENP samples for 2 hr, and acute cytotoxicity was evaluated by determining the percentage of live cells in the culture. Figure 3.7 shows the percent live cells after the 2 hr exposure to each HfO_2 batch. Batch 1 showed the highest levels of cytotoxicity to the HaCaT cells, causing almost a 50% decrease in live cells at a HfO_2 concentration of 2000 ppm. Batches 2, 3, and Micron only showed significant toxicity at high concentrations. Batches 2 and 3 only decreased live cells by approximately 10% at 2000 ppm compared to the control. The Micron batch was only significantly toxic at the highest concentration tested, 5000 ppm, showing a 25.7% relative decrease in live cells.

These results show that for HfO_2 particles, size is not a good predictor of cytotoxicity. Since batch 3 HfO_2 particles had the smallest size, their lack of cytotoxicity was unexpected. Also, batch 1 HfO_2 particles, which had the largest measured diameter, were clearly the most cytotoxic. The increased toxicity of batch 1 may be attributed to different surface contaminants. As part of the SRC collaborative effort to investigate these HfO_2 particles, Dr. Buddy Ratner performed ToF-SIMS analysis on each batch of HfO_2 particles in order to

evaluate surface contaminants that might be affecting toxicity. Since the particle batches came from different manufacturers, differences in contamination may arise due to different synthesis routes or environments that the particles are stored. The main finding from the ToF-SIMS analysis was that batch 1 HfO_2 particles showed a higher intensity bromine contamination than the other batches, possibly resulting from the synthesis pathway, which commonly uses $HfBr_4$ as a starting material. These high bromine levels may have contributed to the higher toxicity levels observed for batch 3 HfO_2 particles (Field et al., 2011).

To determine if the HfO_2 ENPs have similar effects on 16HBE14o- cells as on HaCaT cells, a Live/Dead assay was performed on 16HBE14o- cell cultures exposed to batch 3 HfO_2 for 2 hr (Figure 3.8). Consistent with the HaCaT results, only slight cytotoxicity was induced at the highest concentration tested, 2000 ppm HfO_2, demonstrated by a decrease in live cells by only 8% compared to the control.

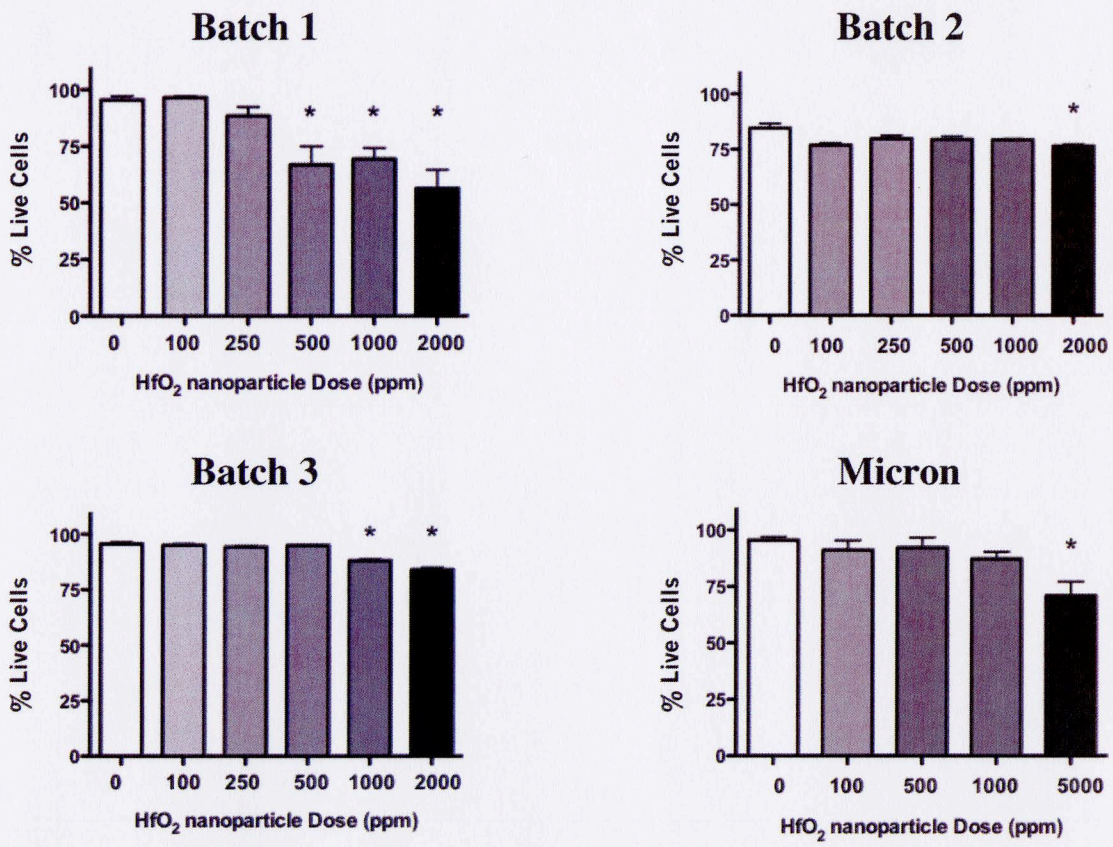

Figure 3.7: Live/Dead cytotoxicity assay on HfO_2 batches shows minimal cytotoxicity to HaCaT cell cultures. HaCaT cells were cultured in 24-well plates in full growth medium and grown to confluence. Cell monolayers were exposed to appropriate concentrations of HfO_2 in HBSS for 2 hr at 37°C. Batch 1 HfO_2 exhibited the greatest toxicity, with a significant decrease in percentage of live cells at 500 ppm HfO_2. Batches 2, 3, and Micron showed minimal toxicity only at the highest concentrations tested. Error bars represent SEM; * represents significantly different than the control culture exposed to HfO_2-free HBSS ($n = 4$, $P < 0.05$).

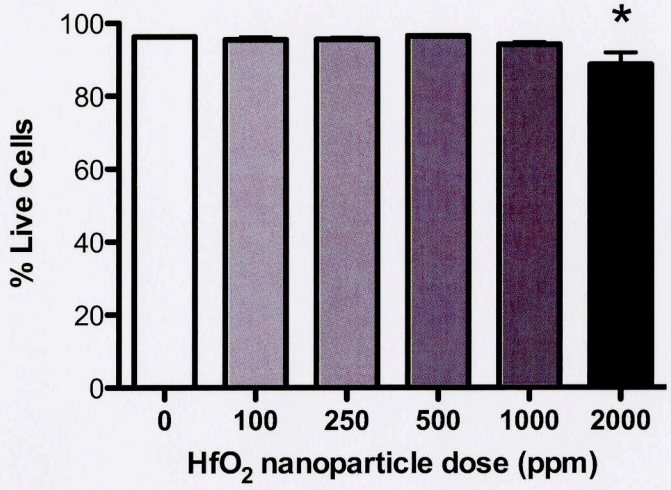

Figure 3.8: Batch 3 HfO_2 ENPs are not cytotoxic to 16HBE14o- cells. 16HBE14o- cells were cultured in 24-well plates in full growth medium and grown to confluence. Cell monolayers were exposed to appropriate concentrations of HfO_2 in HBSS for 2 hr at 37°C. Minimal cytotoxicity was demonstrated towards 16HBE14o- cells, similar to batch 3 HfO_2 toxicity towards HaCaT cells (Figure 3.5). Error bars represent SEM; * represents significantly different than the control culture exposed to HfO_2-free HBSS ($n = 4$, $P < 0.05$).

3.3.2 Real time cell analysis cytotoxicity assay development

Although the Live/Dead assay is effective for evaluating toxicity at a single time point, it is more beneficial to assess cellular responses to ENPs over extended periods of time. Live/Dead assays yield important information on cytotoxicity at single time points that are chosen for comparison studies. RTCA can improve on this approach by continually monitoring changes in cytotoxicity over extended times, up to 48 hrs. Thus, we repeated our ENP cytotoxicity assays using the RTCA device. Prior to performing RTCA toxicity assays, it was

necessary to determine the most appropriate medium and culture conditions in which to run the experiments.

3.3.2.1 Initial cell density affects the rate of proliferation to a cell monolayer

Cell cultures exposed to ENPs in the RTCA cytotoxicity assay were grown to ~80% confluence before ENP exposure in order to best represent an epithelial monolayer while allowing for continued growth and measurement during and after ENP exposure. The number of cells initially seeded on the RTCA E-plate influences the proliferation rate of the cells and the time that the culture becomes a confluent epithelium. We took advantage of the RTCA assay to monitor cell proliferation and determine a proper seeding density in which the cell index neither plateaus, nor increases too slowly, and forms a confluent monolayer within 24 hrs. To determine the most appropriate initial cell seeding density, a varying number of HaCaT cells (15,000; 20,000; or 40,000 cells/well) were plated, and cell index was monitored over time (Figure 3.9). An initial HaCaT cell density of 40,000 cells/well showed the greatest proliferation rate, and cell index reached a plateau after approximately 8 hrs. Initial densities of 15,000 and 20,000 cells/well had slower growth rates and continued to increase cell index even after 16 hrs. A density of 20,000 HaCaT cells/well was chosen for cytotoxicity experiments because it allowed cell index to near to confluence (~80% of the cell index plateau) in a reasonable time (~16 hrs).

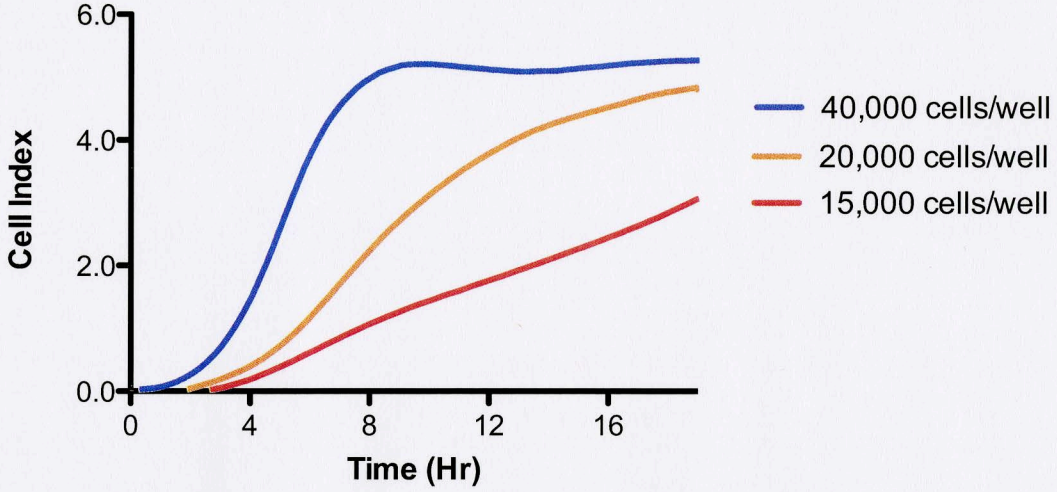

Figure 3.9: Initial HaCaT cell seeding densities on E-plates for RTCA analysis affect proliferation rate. HaCaT cells were plated on 96-well E-plates at densities of 15,000; 20,000; or 40,000 cells/well in full growth medium. The initial cell density of 40,000 cells/well showed the fastest growth rate of the tested initial densities, reaching a plateau at approximately 8 hrs.

Since different cell lines grow at different rates, an appropriate initial cell plating density for one cell type will not necessarily be appropriate for another. Therefore, a similar cell density experiment was also carried out for 16HBE14o- cells, which were used as a model to investigate the cytotoxicity of ENPs on the airway epithelium. 16HBE14o- cells plated at a density of 100,000 cells/well increased faster than those plated at cell densities of 75,000 and 50,000 cells/well (Figure 3.10). In order to mimic the wash and time point at which ENPs are applied to the cell cultures in a cytotoxicity experiment and to determine if washing on a buffer or ENP suspension medium affected the cell index, the cells were washed with HBSS without ENPs after ~20 hrs of proliferation. Following

the HBSS wash, there was a small increase in cell index, which then quickly recovered. The cell index of wells plated with 100,000 and 75,000 cells/well continued proliferating for ~5 hr, and then reached a steady plateau (after ~25 hrs), indicating a steady impedance state likely reflective of decreased proliferation without cell detachment. 16HBE14o- cells seeded at 50,000 cells/well showed minimal proliferation after the HBSS wash and experienced a slight decline in cell index ~40 hrs. Based on these results, we concluded that 16HBE14o- cells plated at 100,000 cells/well will reach an appropriate confluence for a RTCA cytotoxicity experiment in less than 24 hrs.

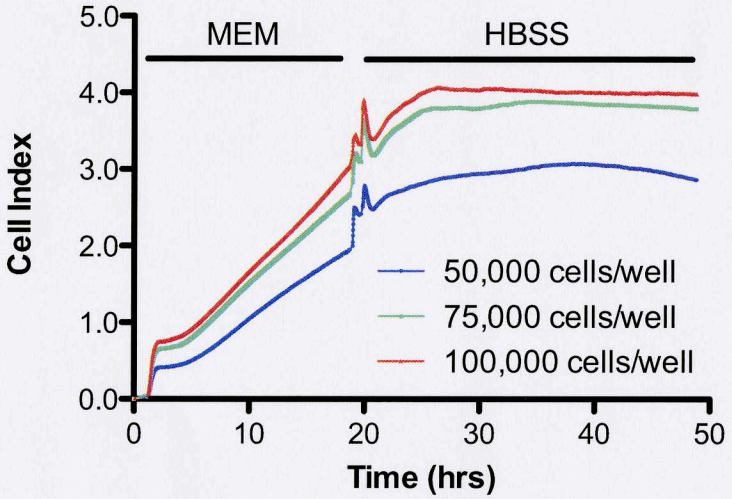

Figure 3.10: Initial cell number affects cell proliferation rate and cell index stability after washing. 16HBE14o- cells were plated on 96-well E-plates at densities of 50,000; 75,000; or 100,000 cells/well in full growth medium. At ~20 hr after plating, growth medium was replaced with HBSS. Initial cell densities of 75,000 and 100,000 cells/well showed increased proliferation rates compared to 50,000 cells/well and more stability of cell index after HBSS wash.

3.3.2.2 ENP suspension medium affects the cell index

ENPs may act differently (e.g. alter agglomeration characteristics) in different suspension media. Therefore, buffers other than HBSS may be required for the optimum ENP suspension and delivery to the epithelial monolayer. We performed a series of experiments to determine if varying the suspension medium affected the cell culture. 16HBE14o- cells have been shown to be stable after washing with HBSS (Figure 3.10). However, if a different buffer (e.g. PBS) provides a more stable dispersion for the ENP, it should be tested for adverse effects on the cell culture as well. The cell index of 16HBE14o- cultures was monitored before and after being washed with either HBSS or PBS. 16HBE14o- cells washed with HBSS maintained a steady cell index, whereas the cell index of those washed with PBS showed a large initial decline due to the PBS wash, and further decreased cell index after ~5 hrs after washing (Figure 3.11A). Therefore, although PBS may provide a good dispersion medium for ENPs, it is not a good choice for the RTCA cytotoxicity assay. A similar experiment was performed on HaCaT cells to compare the RTCA response to buffer washes between cell types. A similar trend was seen in that the PBS wash caused a large decrease in cell index. However, the HBSS wash also caused a decrease in cell index, although not as great as the PBS wash (Figure 11B).

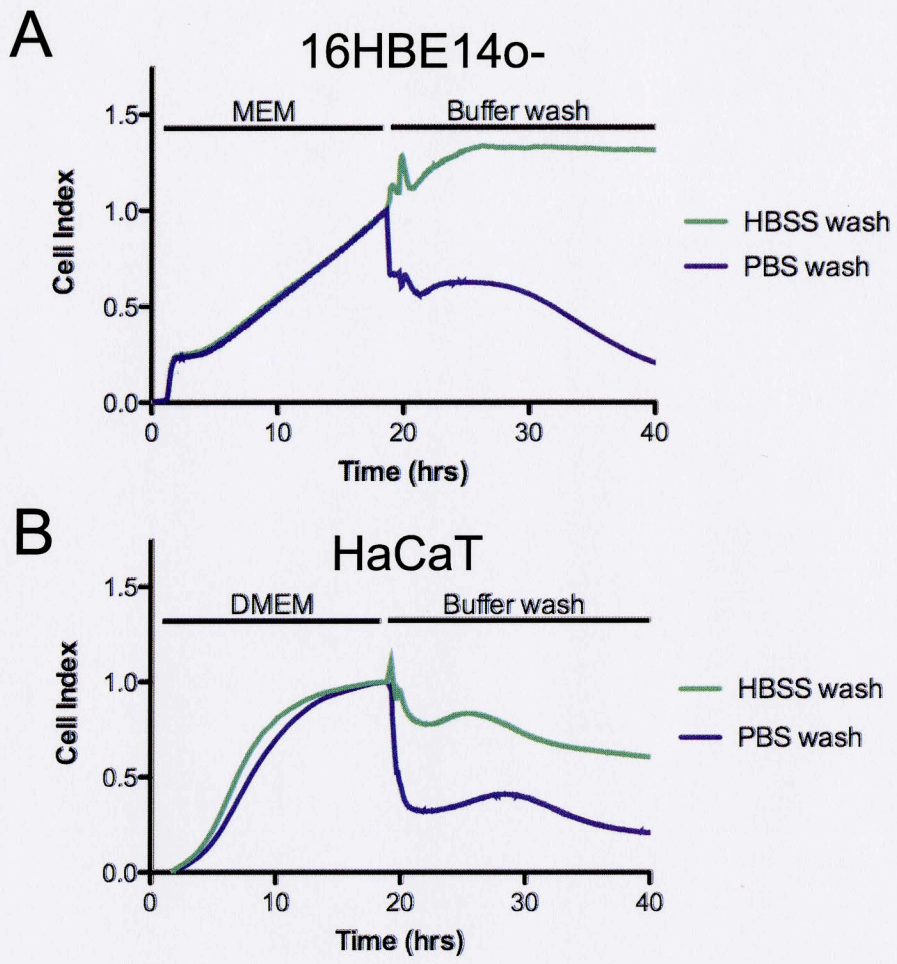

Figure 3.11: Cells washed with HBSS maintain cell index better than cells washed with PBS. Cells were plated on E-plates in full growth medium and allowed to grow for ~20 hr. Cells were washed with either HBSS or PBS solutions and cell index was monitored for an additional 20 hr. (A) 16HBE14o- cells washed with HBSS maintained a stable cell index, while those washed with PBS showed an large initial loss of cell index and a further decline at ~30 hr. (B) HaCaT cells also showed a large decrease in cell index due to PBS wash. An HBSS washed caused a slight cell index decline to HaCaT cells as well.

3.3.2.3 Use of growth medium as an ENP suspension medium

If the cells are allowed to proliferate to a confluent epithelium, and then the ENPs are administered in a suspension medium that is growth medium (instead of a buffer), the cell cultures would not experience the stress of changing media types. In addition to reducing stress to the cells, applying ENPs in growth medium would allow for an prolonged cytotoxicity assay, since the cells would be supplied the proper nutrients. However, since full growth medium contains serum (protein supplementation), ENP-protein interactions can lead to differences in dispersion and agglomeration of the ENPs within the medium, which could affect the potential toxicity effects. To first see if the presence or absence of serum in growth medium (MEM) affected cell growth, the growth medium was replaced after the initial proliferation with either the same full growth medium (supplemented with 10% FBS) or serum-free medium. Both groups of cells continued to show increasing cell index, although cells washed with growth medium without serum had a slightly slower growth rate that developed after 6-8 hrs of medium exchange (Figure 3.12). For the first 6-8 hours after medium exchange, there was no significant difference between full and serum-free medium. Therefore, serum-free growth medium can be used as an ENP suspension medium to reduce the stress imposed on the cells and to extend the length of the experiment, as well as reducing the occurrence of ENP-protein interactions. Furthermore, the average hydrodynamic size of the HfO_2 ENPs is

reduced when dispersed in a growth medium, compared to an HBSS dispersion (Figure 3.4), which is beneficial for assessing the toxicity of the particles.

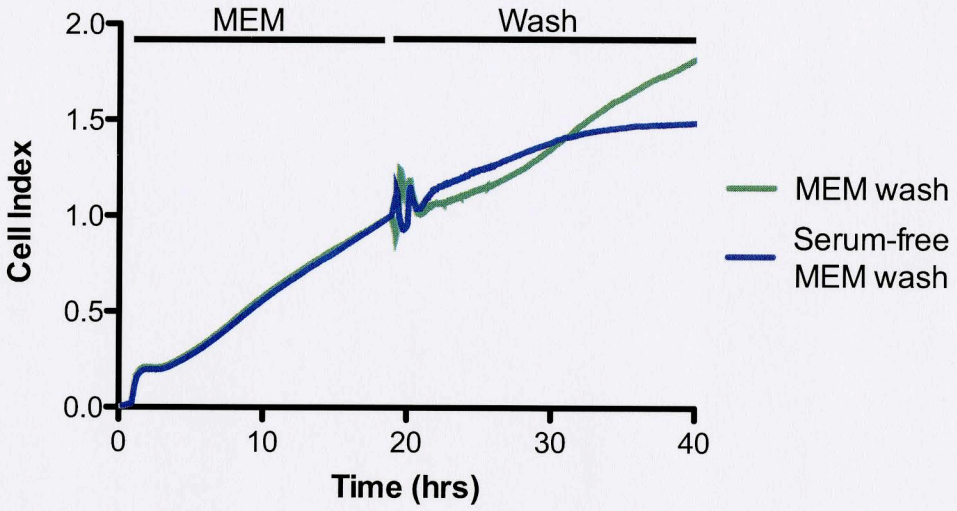

Figure 3.12: Cells washed with growth medium without serum continue to increase cell index, albeit at a slightly slowed rate. 16HBE14o- cells were plated on E-plates in full growth medium at a density of 100,000 cells/well and allowed to grow for ~20 hr. After ~20 hr, cells were washed with either full growth medium supplemented with 10% FBS or serum-free growth medium. Cell index was monitored over time for ~25 hr. Cells washed with growth medium supplemented with serum and cells washed with serum-free growth medium continued to show an increasing cell index over the 25 hr monitoring time.

3.3.3 Evaluation of HfO_2, CeO_2, and SiO_2 cytotoxicity with RTCA

Once parameters for an RTCA cytotoxicity assay were determined, RTCA was used to evaluate the toxicity of HfO_2 batches 1 and 3 (Table 1) to 16HBE14o- cell cultures. Batch 1 was chosen due to its high levels of toxicity

seen in the Live/Dead assay, and batch 3 for its near-nanoparticle average size (150 nm). We found that batch 1 HfO_2 ENPs induced significant cytotoxicity in 16HBE14o- cells at doses of 300 and 500 ppm, as indicated by a decreased cell index. The cell index of cells exposed to 100 ppm batch 1 HfO_2 did not vary significantly from the control (Figure 3.13A). These results agree with the findings of the Live/Dead assay, which assessed cytotoxicity after 2 hrs and showed significant toxicity when cells were exposed to 500 ppm batch 1 HfO_2. Finally, we found HfO_2 ENPs from batch 3 were not cytotoxic when applied at doses up to 5000 ppm (Figure 3.13B). This is consistent with the lack of toxicity seen in the Live/Dead assay. Once again, we found the batch 3 HfO_2 particles (average DLS size, 150 nm) did not induce more cytotoxicity than the larger batch 1 HfO_2 particles (average DLS size, 286 nm). Therefore, we conclude there is not a direct correlation linking smaller ENP size to greater levels of cytotoxicity. However, the cell index traces of cells exposed to 3000 and 5000 ppm batch 3 HfO_2 show a sharp increase compared to the control during the first 10 hrs, which is then recovered to the level of the control. This cell index increase due to high levels of HfO_2 exposure is indicative of a cellular response (i.e. increased cell signaling), and should be investigated in future experiments.

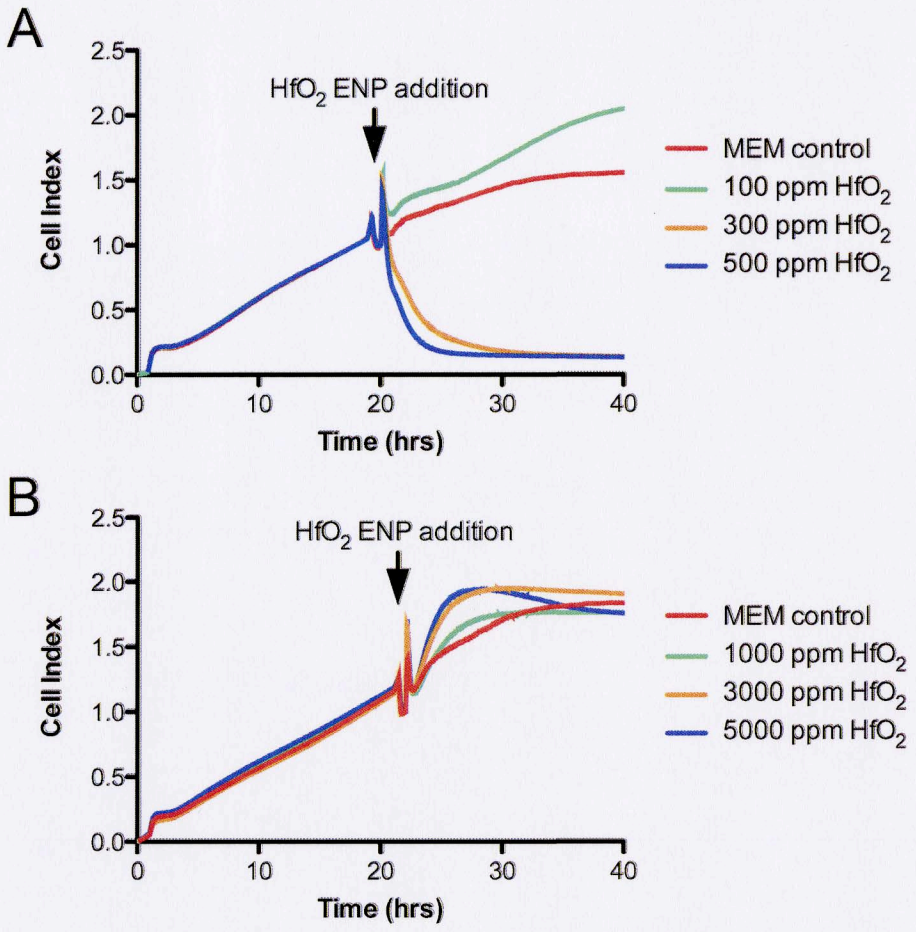

Figure 3.13: HfO_2 batches 1 and 3 show different cytotoxicities. 16HBE14o- cells were plated at a density of 100,000 cells/well and allowed to proliferate ~20 hr. Cells were washed with serum-free growth medium, exposed to appropriate concentrations of HfO_2, and cell index was monitored over time. (A) Batch 1 HfO_2 showed a decreased cell index indicative of cytotoxicity for 300 and 500 ppm (B) Batch 3 HfO_2 did not show decreased cell index for even the highest concentration tested (5000 ppm HfO_2).

In addition to comparing cytotoxicity between HfO_2 ENP batches, toxicity was compared among other ENPs as well, under identical conditions. SiO_2 and CeO_2 were tested for cytotoxicity to 16HBE14o- cells with RTCA analysis. Similar to batch 3 HfO_2 ENPs, CeO_2 ENPs did not induce cytotoxicity at any of

the doses tested (Figure 3.14A). SiO_2 ENPs, however, induced significant toxicity in 16HBE14o- cells at doses of 200 ppm SiO_2 and greater, as indicated by decreased cell indices compared to the control (Figure 3.14B).

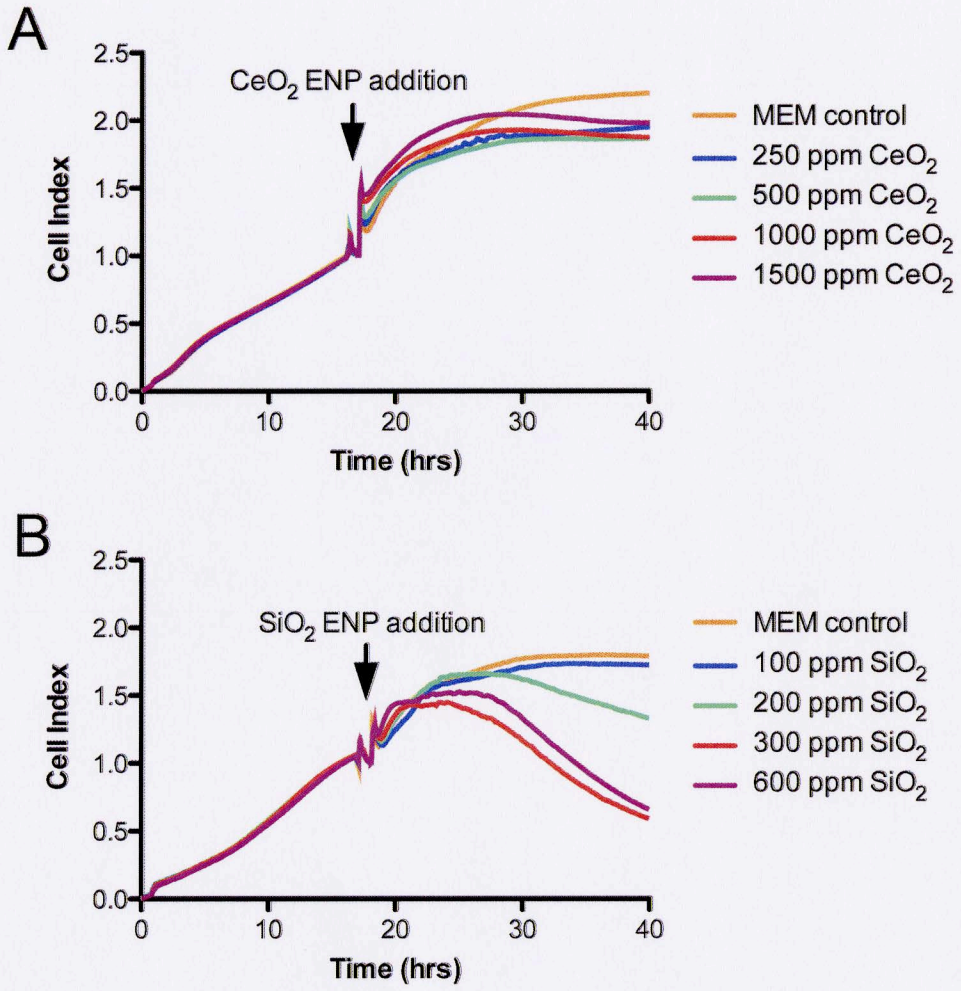

Figure 3.14: SiO_2 ENPs are cytotoxic and CeO_2 ENPs are not. 16HBE14o- cells monitored by RTCA were allowed to proliferate, and then exposed to CeO_2 or SiO_2 ENPs ~20 h. (A) Cells exposed to CeO_2 ENPs continued to grow, and all concentrations tested showed minimal deviation from the control. (B) SiO_2 ENPs demonstrated significant toxicity to cells at concentrations of 200 ppm and greater. Data obtained by Lila Otero Gonzalez, University of Arizona.

3.4 Effect of non-cytotoxic HfO_2 on ATP signaling

Since the ENPs examined induced minimal cytotoxicity (i.e., cell death) in 16HBE14o- cells, and only at relatively high concentrations compared to ENPs that cause toxicity effects at concentrations under 100 ppm (Park et al., 2008), we next focused on how the ENPs might be affecting cellular signaling. The rationale behind these experiments is that although ENP exposure does not kill the cells, it may still interrupt and affect important cell signaling parameters, and thus have an adverse impact on cell function. For example, nanoparticle exposure has been shown to alter innate immune responses in the lung (Inoue, 2011). Purinergic ATP signaling is an important part of the innate immune defenses of the airway epithelium. Local release of ATP can contribute to coordinating many diverse innate immune processes in the conducting airway, including ciliary beat, salt and water transport, and wound repair. Each of these processes can be downstream of ATP-induced Ca^{2+} signaling in airway epithelial cells. Therefore, we examined the effect of low, non-toxic concentrations of ENPs on the airway epithelial response to ATP using both RTCA and Ca^{2+} imaging. Because batch 3 HfO_2 particles did not cause toxicity to airway epithelial cells in the RTCA assay, even at high exposure concentrations (Figure 3.13B), we used these particles to model non-toxic exposures.

3.4.1 RTCA assay shows exposure to HfO_2 attenuates cellular response to ATP

The RTCA assay was adapted to investigate the cellular response of 16HBE14o- cells to exogenously applied ATP. After initial proliferation, cells were exposed to varying doses of batch 3 HfO_2 (0 ppm, 50 ppm, or 250 ppm) for 24 hrs. Cells grown in HfO_2-free and HfO_2-supplemented growth medium displayed similar cell index traces over the 24 hr exposure (Figure 3.15), which demonstrated these doses were non-cytotoxic and in agreement with the lack of cytotoxicity established by the fluorescent Live/Dead assay (Figure 3.8) and RTCA toxicity assay (Figure 3.13B).

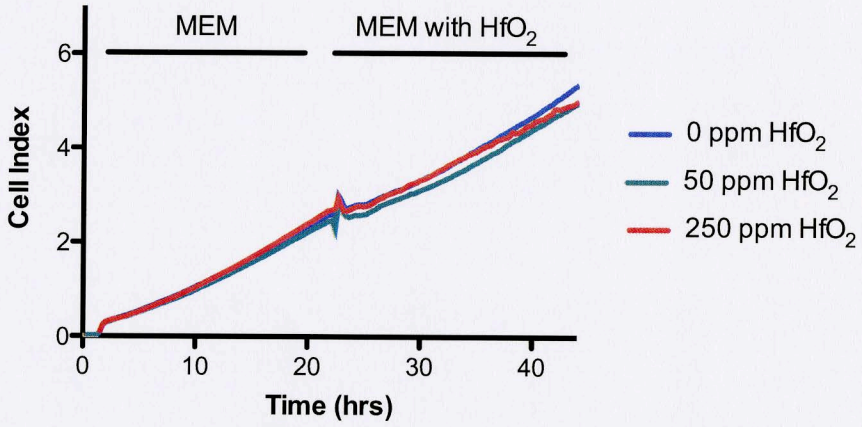

Figure 3.15: Low doses of HfO_2 batch 3 do not affect cell growth over 24 hr exposure. 16HBE14o- cells were grown in MEM, which was replaced after ~23 hr with batch 3 HfO_2 supplemented MEM (50 or 250 ppm). Cell index traces show that cell growth is not affected by 24 hr exposure to batch 3 HfO_2 compared to the 0 ppm control.

After the 24 hr exposure, ATP was exogenously applied to the cells in varying doses (100 nM to 100 μM in ½ log steps) and caused a rapid, dose-dependent increase in cell signaling as shown by a rapid increase in cell index (Figure 3.16A). 16HBE14o- cells exposed to both 50 ppm and 250 ppm batch 3 HfO_2 showed a diminished response to the applied ATP, seen by comparing both the peak response and the continued response over the 4 hr experiment (Figure 3.16B, C). Dose response curves based on cumulative response were calculated from the area under the curve. The response to ATP of cells exposed to HfO_2 was significantly reduced (Figure 3.16D).

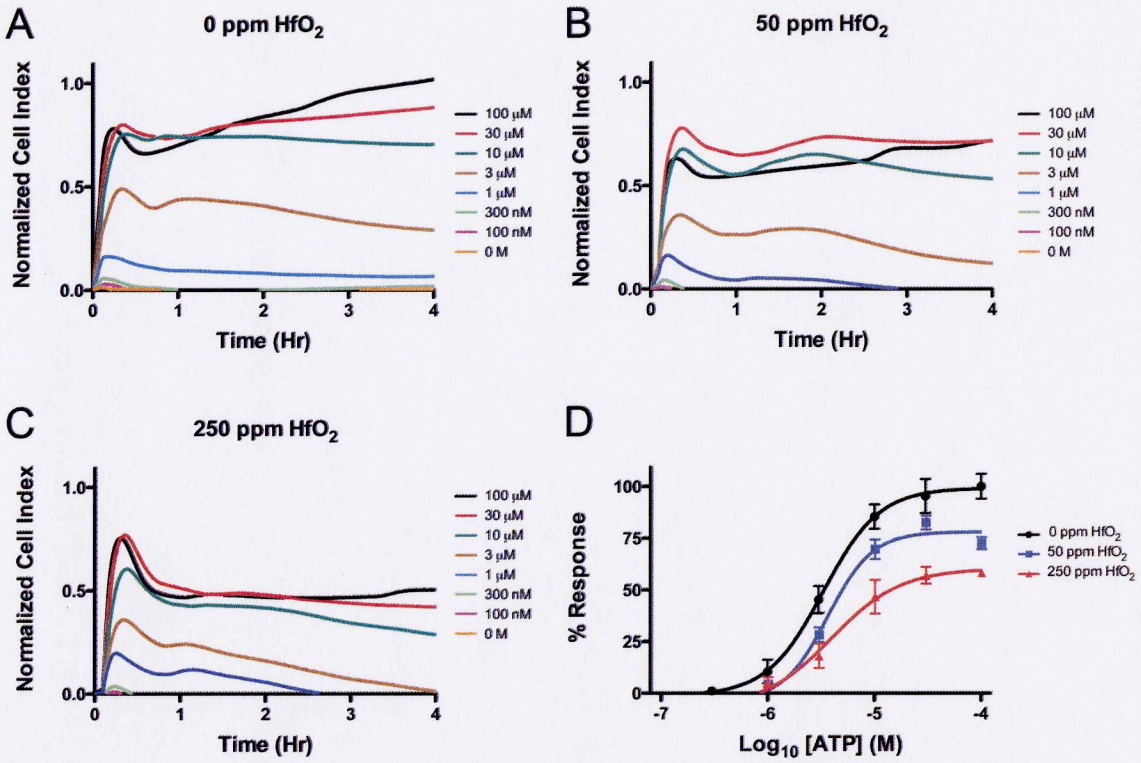

Figure 3.16: Exposure to non-cytotoxic levels of HfO_2 dampens cellular response to ATP. 16HBE14o- cells plated on E-plates were allowed to grow ~20 hr, then exposed to 0, 50, or 250 ppm batch 3 HfO_2 in full growth medium for an additional 24 hours. ATP (0 – 100 µM in ½ log steps) was added to individual wells (shown as time 0; n=4 for each dose), and cell index was monitored over time. (A) ATP addition caused a rapid, dose dependent increase in cell signaling, which was (B) attenuated by exposure to 50 ppm batch 3 HfO_2 and (C) 250 ppm batch 3 HfO_2 relative to the control. (D) Total integrated cellular responses for each HfO_2 exposure concentration were calculated from the area under the curve for the 4 hr experiment for each ATP dose (n=4) and plotted as percent of maximum response (i.e., the value at 0 ppm HfO_2 and 100 µM ATP) to obtain a dose response curve. Fitted curves are shown for comparison. Both 50 and 250 ppm HfO_2 exposures significantly reduced the response to ATP (two-way ANOVA; $P < 0.0001$).

3.4.2 HfO_2 exposure reduces the Ca^{2+} response of human epithelial monolayers to exogenously applied ATP

Application of exogenous ATP to airway epithelial cells can induce activation of many signaling systems, including the increase of $[Ca^{2+}]_i$ in human airway epithelial cells. To evaluate if airway epithelial cells exposed to ENPs have an altered Ca^{2+} response, we monitored $[Ca^{2+}]_i$ following exogenous ATP addition with digital imaging microscopy (Figure 3.17) (Sherwood et al., 2011). In 16HBE14o- cultures that were not exposed to ENPs, ATP application induced a rapid increase in $[Ca^{2+}]_i$ over the entire field of view, with approximately 44% of cells reaching a $[Ca^{2+}]_i$ threshold level of 200 nM. Cell cultures exposed to non-cytotoxic concentrations of HfO_2, SiO_2, and CeO_2 ENPs for 24 hrs prior to ATP application showed a reduced response to ATP application compared to the control, with significantly fewer cells in the field of view reaching the 200 nM $[Ca^{2+}]_i$ threshold (Figure 3.18A,B,C). Of the ENPs tested, exposure to SiO_2 ENPs caused the greatest decrease in $[Ca^{2+}]_i$ response, with 71% fewer cells responding after exposure to only 10 ppm CeO_2, and 91% fewer cells responding after exposure to 25 ppm CeO_2 (Figure 3.18C). Exposure to SiO_2 ENPs also caused significant reduction in $[Ca^{2+}]_i$ response following exposure, showing only 50% response compared to the control (Figure 3.18B). HfO_2 ENPs also affected the $[Ca^{2+}]_i$ response to ATP, although significant differences were only seen at 25 ppm exposures (Figure 3.18A).

Our studies showed that neither the nano-sized HfO_2 nor the micron-sized HfO_2 was significantly cytotoxic (i.e., caused cell death) to our cell cultures, indicating that smaller particle size does not directly relate to increased toxicity or biological effects. However, we hypothesized that smaller particles could have a greater effect on Ca^{2+} signaling than larger particles have. Therefore, we exposed 16HBE14o- cells to reference micron-sized particles of the same concentrations and 24 hr exposure time, and examined their $[Ca^{2+}]_i$ response to ATP. Cell cultures exposed to the micron-sized HfO_2, SiO_2, and CeO_2 particles still demonstrated reductions in $[Ca^{2+}]_i$ response relative to the control following a 24 hr exposure, although to a lesser extent than nano-sized particle exposure. SiO_2, especially, did not cause a significant reduction in $[Ca^{2+}]_i$ response even after 25 ppm exposure (Figure 3.18E). However, micron-sized HfO_2 and CeO_2 particles did both cause significant reductions in Ca^{2+} signaling after exposure to concentrations of 50 and 25 ppm, respectively, showing that both micron- and nano-sized particles can reduce the Ca^{2+} signaling response to ATP (Figure 3.18D, F).

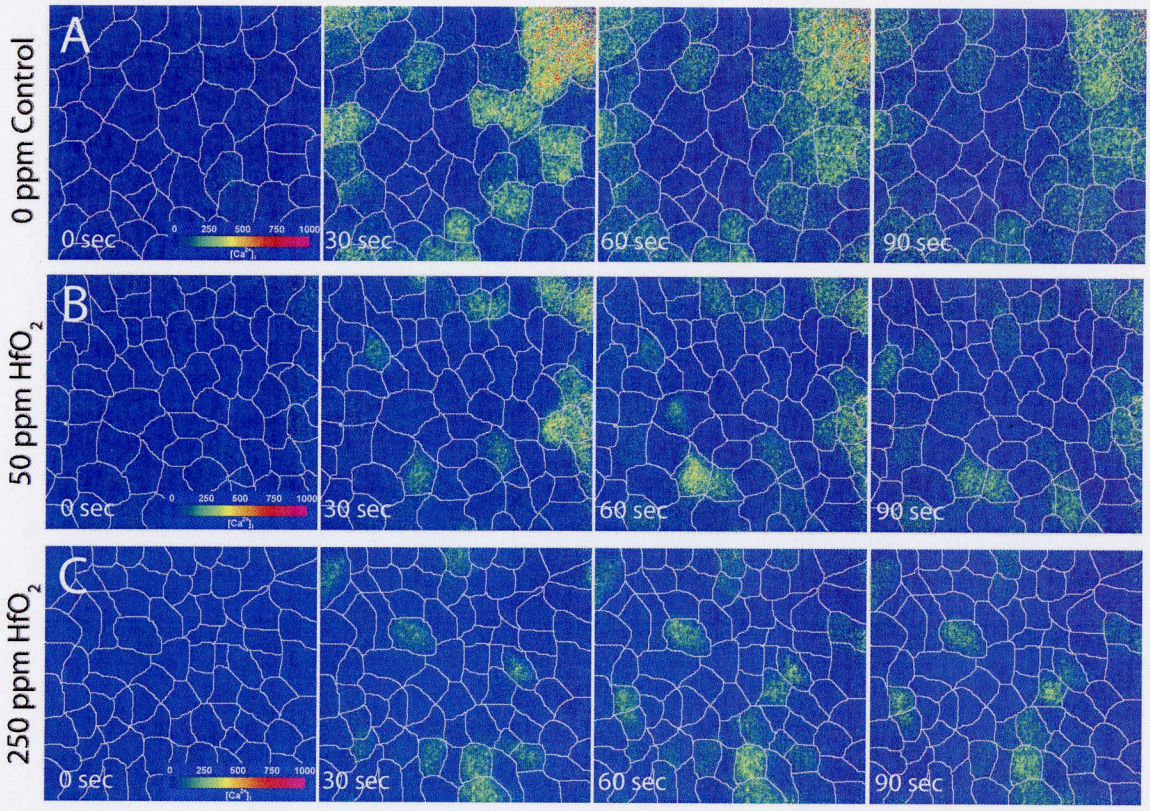

Figure 3.17: Nano-HfO_2 particles reduce ATP-induced Ca^{2+} response in human airway epithelial cells, visualized by single viewing fields of cells from cultures treated with or without HfO_2 and monitored over time (3 min) for $[Ca^{2+}]_i$ changes after the addition of 1 μM ATP. 16HBE14o- monolayers were grown to confluence on coverslips. Cell monolayers were exposed to HfO_2-free or HfO_2-supplemented growth medium (50 or 250 ppm) for 24 hrs and subsequently monitored for $[Ca2+]_i$ changes in response to application of 1μM ATP. Panels (B) and (C) show reduced $[Ca^{2+}]_i$ changes compared to the control shown in panel (A). White lines approximate cell borders. The time following ATP wash is in the lower left of boxes. The color scale for $[Ca^{2+}]_i$ is shown in the 0 sec time point of each panel. Results are quantified in Figure 3.18.

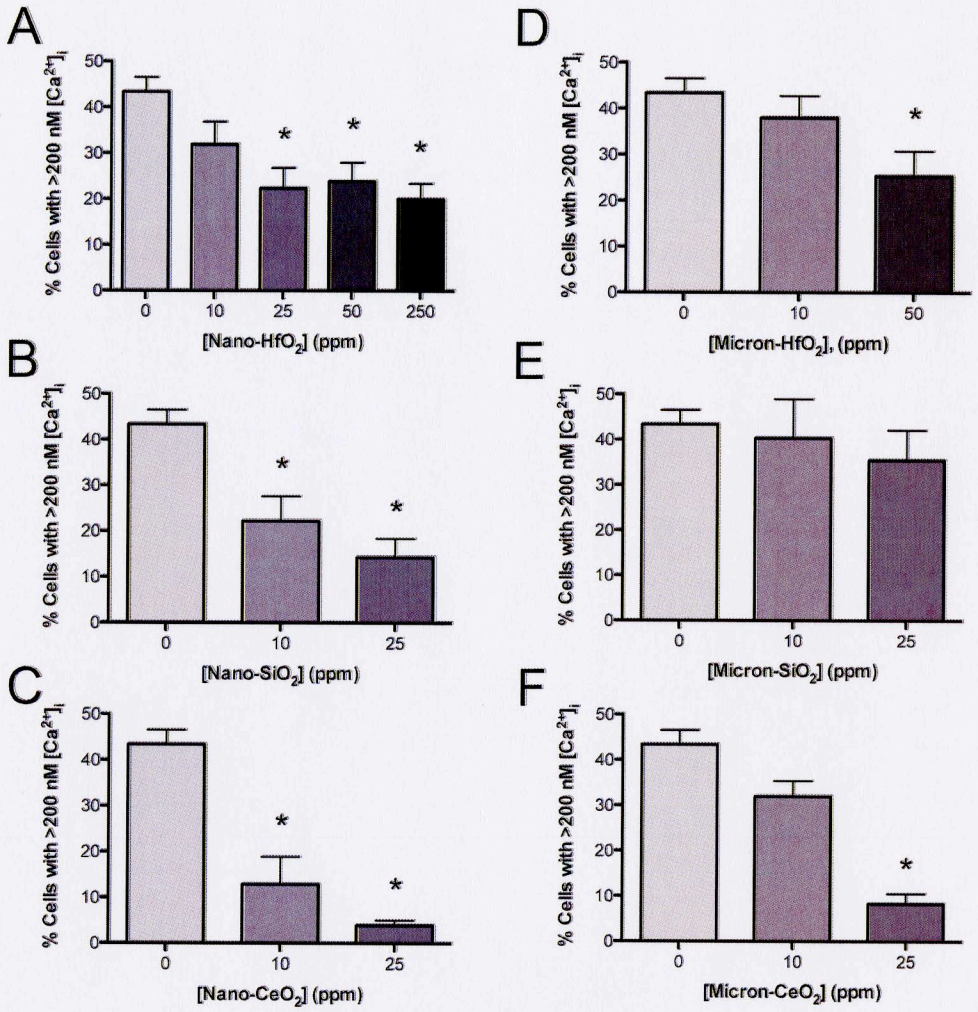

Figure 3.18: ENP exposure reduces ATP-induced Ca^{2+} response in human airway epithelial cells. 16HBE14o- monolayers were grown to confluence on coverslips. Cell monolayers were exposed to ENP-free or ENP-supplemented growth medium (varying from 10 to 250 ppm) for 24 hrs and subsequently monitored for $[Ca2+]_i$ changes in response to application of 1μM ATP. Cell monolayers exposed to ENPs demonstrated a lower percentage of cells responding (by increasing $[Ca2+]_i$ to >200 nM) to ATP. Graphs show percentage of cells responding to ATP with an increase in $[Ca2+]_i$ to >200 nM for 24 hr exposure to (A) nano-HfO_2, (B) nano-SiO_2, (C) nano-CeO_2, (D) micron-HfO_2, (E) micron-SiO_2, and (F) micron-CeO_2. Error bars represent SEM; * indicates significantly different than control culture ($P < 0.05$).

3.4.3 Examining mass and surface area concentration dose-metrics

Because defining the most appropriate dose metric of ENPs remains a challenging issue in nanotoxicology, we more closely examined the doses administered to the cell cultures in the previous experiments. An interpretation of size-dependent biological responses to ENPs depends on the choice of dose metric used for comparison. Examples of nominal dose metrics that have been studied are particle mass, particle number, and surface area doses. Since for a given mass of particles, the total surface area increases with decreasing particle diameter, we hypothesized that the surface area concentration administered to the cells would better be a better predictor of ENP exposure effect than the mass concentration dose. Therefore, we examined the results from Ca^{2+} imaging of 16HBE14o- cell cultures after 24 hr exposure to nano- and micron-sized particles (Figure 3.18) on both mass and surface area bases (Figure 3.19). Mass concentrations were converted to surface area concentrations with the following relationship:

$$\text{Surface area concentration} = \frac{\text{mass concentration}}{\text{density}} \bullet \frac{6}{d} \qquad (1)$$

where surface area concentration is in cm^2/ml media, mass concentration is in g/ml media, density is in g/cm^3, d is the average hydrodynamic particle diameter in cm (measured by DLS or diffraction, Tables 1 and 2), and particles are assumed to be spherical. Conversions were examined for HfO_2 and SiO_2 particles because size measurements were available for both nano- and micron-

sized particles. A particle size measurement was not determined for the micron-sized CeO_2 particles and therefore an accurate surface area concentration could not be determined.

For comparison between mass and surface area dose metrics, the Ca^{2+} responses to 1 μM ATP (Figure 3.18) were plotted against both dose metrics. When Ca^{2+} responses are plotted versus administered mass concentration, nano-sized particles cause greater reductions in Ca^{2+} response for a given mass compared to micron-sized particles (Figure 3.19A,B). However, when plotted on a surface area basis, a logarithmic relationship develops (Figure 3.19C,D). Ca^{2+} response decreases as total surface area increases, indicating that surface area could be an important determinant of toxicity.

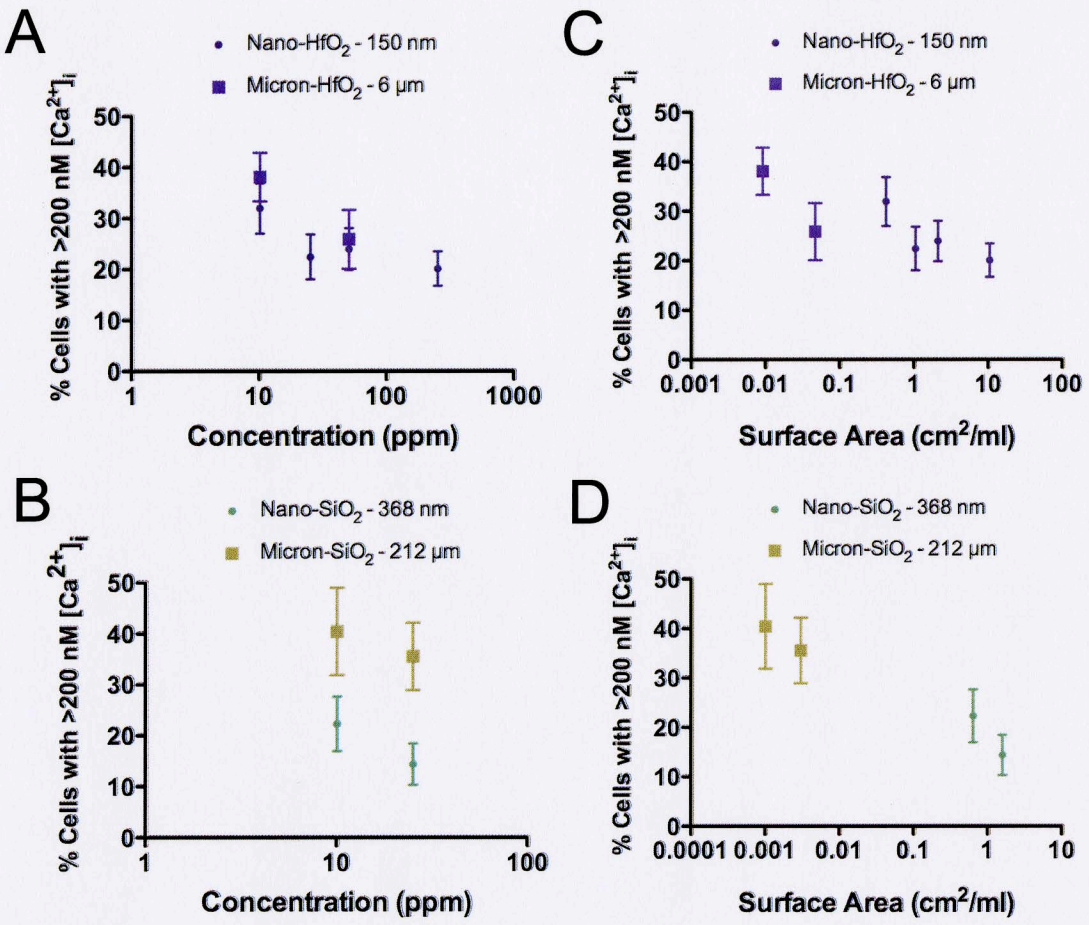

Figure 3.19: Comparison of mass and surface area concentration dose metrics. Ca^{2+} responses to 1 µm ATP of 16HBE14o- cell cultures exposed for 24 hrs to varying mass concentrations of (A) HfO_2 and (B) SiO_2. The same responses are plotted against corresponding surface area concentrations for (C) HfO_2 and (D) SiO_2, calculated based on the assumption of spherical particles and equation 1.

3.4.4 Examining particle deposition based on sedimentation and diffusion

Instead of exposure dose administered to the cell culture, a target tissue paradigm for dosimetry has been proposed to improve the accuracy and predictive power of *in vitro* systems for assessing ENP hazards (Hinderliter et al.,

2010). The *In vitro* Sedimentation, Diffusion, and Dosimetry (ISDD) model provides mathematical calculations that circumvent direct experimental measures of cellular dose, since these can be difficult and expensive. The ISDD model, which was developed in Matlab (MathWorks, Inc.), was obtained from the authors and used to examine the *in vitro* target cell dose of our tested ENPs that was transported to cells in culture over the duration of exposure. In order to determine the fraction of particles transported from media to the bottom of the culture well, the ISDD model uses the principles of diffusional and gravitational transport of particles in viscous media. Inputs of temperature, media density and viscosity, medium height, hydrodynamic particle size in the test media, and particle density allow the model to produce a time-course of particle transport, and ultimately the fraction of particles delivered to the cells over time.

We used the ISDD model to look at the time-course of particle delivery to the cell culture in order to determine if there were differences in the delivered particle dose between the ENPs we examined (Figure 3.20). The model showed that of the ENPs tested, SiO_2 (368 nm) takes the shortest amount of time, ~2.5 hrs, to deliver the full administered dose to the cells when exposed in a culture well with surface area of 1.8 cm^2 and media height of ~1.4 mm (Figure 3.20A). However, in all three cases, the full dose was delivered to the cells after ~6 hrs of exposure. Therefore, cells exposed to the ENPs for 24 hrs prior to Ca^{2+} imaging experiments had received the full administered dose.

Additionally, particle fraction deposited over time was calculated for particles administered to cell cultures in 96-well E-plates in order to examine how long it takes particles to reach cells in RTCA cytotoxicity assays. Media height used in RTCA experiments is ~10.2 mm, which is much greater than media heights used in larger wells for cell culture on coverslips (for Ca^{2+} imaging experiments). Since the height of the media above cells in culture determines the distance particles must travel to reach cells, it is a large factor in the determination of the fraction of particles delivered. Increases in media height reduce the fraction of the administered dose reaching cells. Therefore, it is not surprising that for E-plate wells with a higher media height, a longer exposure time is needed to deliver the full administered dose (Figure 3.20B). This is an important consideration when examining cytotoxicity demonstrated by cells exposed to ENPs. Since only fractions of administered doses are delivered during the course of a cytotoxicity experiment, it becomes more difficult to compare dose-response data. The ISDD model could not be used on the micron-sized particles because their measured diameters were too large for the simulations to run.

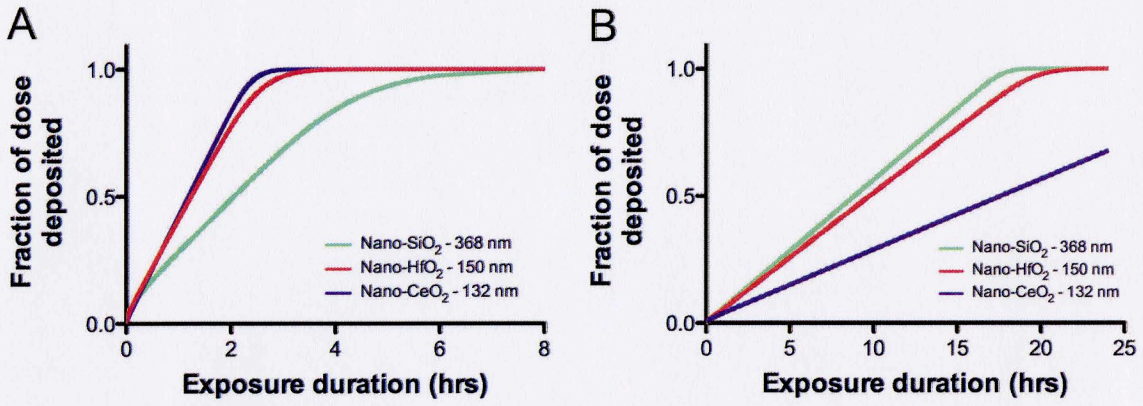

Figure 3.20: Transport rates for tested ENPs during *in vitro* experiments. ISDD calculated fraction of ENPs delivered to cells over the duration of an *in vitro* exposure (A) in cell culture dish wells with surface area of 1.8 cm^2/well and (B) in an E-plate with surface area of 0.196 cm^2/well. Different rates of particle transport result in different time-course for delivery to cells. Calculations were made with ISDD model provided by Hinderliter et al. (Hinderliter et al., 2010).

CHAPTER 4 - DISCUSSION

Currently, there are no exposure limits that address engineered nanoparticles. Nor are there standard measurement techniques for ENPs in the workplace (Methner et al., 2010). In an era of expanding nanotechnologies and widespread production of engineered nanoparticles, ENP hazards must be assessed to protect employers, workers, and researchers that are potentially exposed in facilities where ENPs are produced and/or handled. A first step in establishing human exposure limits is to determine the toxicity of the ENPs. However, toxicology assessments fail to keep up with the fast pace at which new ENPs are produced. An *in vitro* toxicity assay that models inhalation or dermal exposure to ENPs will be beneficial in assessing the hazards of new ENPs. *In vitro* models that can be used to shed light on biological mechanisms for ENP effects are also needed to understand their toxicity. By examining characterized ENPs, this thesis established an RTCA assay to evaluate ENP cytotoxicity both in terms of cell death and decreased cellular response.

A toxicity assay like the one developed in this thesis is key to addressing the growing knowledge gap between emerging sophisticated materials and quantitative toxicology and risk assessment. It is vital to rapidly screen ENPs for potential toxicity and adverse cellular effects before they can be further tested for causing specific cellular alterations or examined *in vivo.* However, there is a range of approaches and methods that have been used to investigate the effects

of manufactured nanoparticles which lead to different results (Oberdorster et al., 2005). This inconsistency indicates a need for standardized tests in order to get comparable results when screening ENPs for toxicity effects. The EPA has recognized this need with their establishment of the Working Party on Manufactured Nanomaterials (WPMN). One project of the WPMN is to develop *in vitro* tests to evaluate ENPs with a responsible and coordinated approach (EPA, 2011). An RTCA cytotoxicity assay like the one we developed can be standardized, quick, and high-throughput. Furthermore, we were able to modify the assay for two different cell types in order to mimic both airway and skin exposure. Therefore, this assay can be standardized to maximize coordination between studies, but is also versatile, in order to investigate various ENP exposure routes.

Additionally, the RTCA assay not only looks at end point toxicity, but it also tracks cellular responses over an extended period of time. This eliminates the need to choose a single exposure time at which to evaluate cytotoxicity. Since the health and activity of the cells is continuously monitored, we gain information about the rate and quantity of cell death, as well as about toxic effects in the absence of cell death. ENP exposure has the potential to cause toxic effects without reaching the "ultimate" end point of cell death in a toxicity experiment. For example, cell transformations or the loss of ability to respond to cellular signals or stress could result from ENP exposure (Nel et al., 2006). In

this thesis, RTCA was used to examine exposure to ENPs that did not cause cell death, but did reduce cellular response to an innate immune signal, ATP.

This RTCA result led us to further investigate the loss of ATP signaling due to ENP exposure. Although a loss of signaling is not "toxic" in terms of cell death, alterations of signaling pathways can contribute to chronic disease and therefore can be detrimental. Since an increase in $[Ca^{2+}]_i$ is part of a signaling pathway downstream from ATP activation, we examined $[Ca^{2+}]_i$ changes in response to ATP. We exposed airway epithelial cells to sub-cytotoxic ENP concentrations and showed that their $[Ca^{2+}]_i$ response to a typical signaling concentration of ATP was reduced. However, since ENP physical and chemical characteristics play a large part in their toxicity effects, it was not surprising that the three ENPs tested (with varying sizes) did not cause identical reductions in signaling. These differences highlight the importance of thorough ENP physical and chemical characterizations that should be carried out when examining the potential adverse effects of ENPs. To fully describe the differences between the particles and gain further understanding of why they can cause different biological effects, we need to accurately characterize the particle surface area, crystal structure, agglomeration status in relevant media, composition and surface coatings, surface reactivity, method of synthesis and post-synthesis modifications, and purity of the sample (Warheit et al., 2009).

A highly debated issue in nanotoxicology is the potential particle size-dependence of ENP toxicity. In order to investigate the hypothesis that smaller

particles induce greater toxicity due to greater biological interactions, we examined the $[Ca^{2+}]_i$ response to ATP on airway epithelial cells exposed to micron-sized particles, much larger in size than the ENPs tested. Although the nano-sized particles did reduce the Ca^{2+} signal at lower concentrations than the micron-sized particles, there was not a direct correlation between sizes. Significant reductions in $[Ca^{2+}]_i$ response to ATP were caused by exposure to micron-sized HfO_2 and CeO_2. Micron-sized SiO_2 particles were the only particles tested that did not significantly affect Ca^{2+} signaling at the concentrations tested. Therefore, we can conclude that the alterations in $[Ca^{2+}]_i$ changes caused by particle exposure are not only based on the size of the particles.

However, one consequence of the small size of nanoparticles is that they have a large total surface area, which can potentially lead to increased biological interactions and therefore larger cellular effects. We examined this hypothesis by relating decreases in $[Ca^{2+}]_i$ responses to ATP to ENP surface area exposures (calculated based on mass concentration, particle density, and measured hydrodynamic size). This showed a toxicity response that was logarithmically related to surface concentration, indicating that toxicity may be better predicted by the amount of ENP surface area exposed to cells, rather than particle size alone.

Another issue related to the dose metrics used to assess ENP toxicity with *in vitro* assays is the affect of solution dynamics, including particle diffusion and sedimentation (Teeguarden et al., 2007). The ENP dose in an *in vitro* system

can be difficult to compare across particle types that have varying densities, shapes, surface properties, and sizes. An assessment of the actual cellular dose exposed to the cells should be considered when evaluating impacts of nominal doses of ENPs. Therefore, we used a computational model to describe the rate at which the ENPs are delivered to the target tissue, based on sedimentation and diffusion (Hinderliter et al., 2010). We found that media height has a high impact on the rate of deposition, indicating that this, as well as other parameters affecting diffusion and sedimentation, should be taken into account when comparing cellular responses across systems.

The current work has shown that sub-cytotoxic concentrations of ENPs have the potential to cause detrimental effects to human airway epithelial cells by reducing the cellular response to ATP. However, ATP signaling can mediate a diverse spectrum of effects in many cell types upon receptor binding (Ahmad et al., 2006). Future work should investigate the receptors that bind ATP (P2X and P2Y) and the specific pathways that may be affected by ENPs. Also, purinergic receptors have been shown to be involved in the cellular response to oxidative stress (Mason et al., 2004), which is often produced by the presence of ENPs (Akhtar et al., 2010; Park et al., 2008). Therefore, the potential link between ENP-caused oxidative stress and altered purinergic signaling should be examined.

CHAPTER 5 - CONCLUSIONS AND FUTURE WORK

A major goal of this work was to examine the cytotoxicity effects of ENPs to cultured human airway epithelial cells. A limitation encountered was that the examined ENPs were not actually in the nano-size range (< 100 nm in diameter). Although the particle sizes of the ENPs used in these studies were reported by the suppliers to be nano-sized, particle diameters measured by DLS and laser diffraction were much larger. This inconsistency limited our conclusions related to ENP toxicity. Although we observed cell death due to SiO_2 particles and reductions in cell signaling due to HfO_2, SiO_2, and CeO_2 particles, we cannot conclude that these affects are due to "nanotoxicity"; but rather, they may result from a metal toxicity. In order to complete this evaluation, future experiments should examine the potential toxicity of true nanoparticles to better assess size-dependent effects.

We can conclude that sub-cytotoxic exposures to engineered particles can alter basic innate immune function in lung epithelial cells, including paracrine response to ATP signaling. Although these particle exposures did not cause cell death, they present detrimental health hazards that simple cell death assays do not reveal. In order to further the studies in this work, the effects of micron-sized particle exposure should be investigated with the RTCA assay in terms of both cell death and reduced ATP signaling. This comparison of micron-size particles to nano-sized particles would help to determine if cytotoxicity and the dampening

of overall signaling response to ATP is related to the particles' nano-size or their metal properties. Furthermore, potential particle interactions with ATP should be examined, since ATP-nanoparticle interactions could potentially limit available ATP and therefore decrease the response. In order to examine the ATP response without opportunity for ATP-particle interaction, the experiments done in this work could be modified. For example, if after a 24 hr ENP exposure, the particles were washed off the cell culture, and then ATP was administered, potential ATP binding to nanoparticles would be avoided. In this way, it could be determined if nanoparticles decrease the ATP signaling response by interfering with ATP or by affecting the cell directly.

Other parameters of nanoparticle cytotoxicity should also be examined. For example, surface charge can affect the internalization of nanoparticles and therefore toxicity. Measuring the zeta potential of the particles is one way to assess the charge surrounding a nanoparticle in solution, and the zeta potential may affect the particle's ability to permeate the cell membrane (Clogston and Patri, 2011). For example, particles with a more positive zeta potential can have a higher tendency to enter cells or disrupt cell membranes, and therefore show greater toxicity. If we measure the zeta potentials of the nanoparticles we are examining (HfO_2, CeO_2, SiO_2,), a relationship between zeta potential and the induced cytotoxicity that we observe could emerge. Furthermore, studies have coated nanoparticles with polymers or functional groups to create particles that are positive, negative, or neutrally charged, but with the same core (e.g. CeO_2),

showing a surface charge-dependent localization that may play a role in the particle's toxicity (Asati et al., 2010; Bhattacharjee et al., 2010). An approach like this could be used to show how the surface charge affects the toxicity of a nanoparticle like HfO_2. Another parameter to investigate that is related to nanoparticle toxicity effects is the presence of free metal ions. For example, toxic effects of Cu nanoparticles are increased due to high copper ion concentrations that result from the high reactivity of Cu nanoparticles (Griffitt et al., 2008). The difference in toxicity may arise from different uptake mechanisms. For example, metal nanoparticles may be too big for ion transporters or paracellular diffusion pathways, but may likely be endocytosed. Metal nanoparticles could also exert toxic effects without uptake into internal organs. In future studies with HfO_2, the effects of nano-metal and dissolved metals should be investigated. To determine if there is a difference in toxicity of nano-metal and dissolved metals, we could examine hafnium in the ionic state using a hafnium salt ($HfCl_4$), and compare the metal salt toxicity to the nanoparticle toxicity.

With these proposed experiments, in combination with the findings of this study, we would be able to better understand the parameters of nanoparticles like HfO_2 that contribute to or enhance toxicity effects. Exposure of airway epithelial cells to HfO_2 particles was shown to cause toxicity in terms of reduced paracrine response to ATP signaling. By examining true nanoparticles alongside the slightly larger particles studied in this work, we would help to elucidate altered

toxic effects due to the differing physicochemical features of nanoparticles. A second important outcome from the experiments discussed above would be a better identification of distinct properties of the particles that are involved in their toxic effects; these include a possible surface charge dependency or a contribution of free metal ions. With these studies, the extremely limited data on HfO_2 toxicity that arises from both nano- and metal-based mechanisms would be enhanced. Further, as a model nanoparticle, this approach and resulting data could provide important information on more commonly used nanoparticles.

REFERENCES

Abassi, Y.A., B. Xi, W. Zhang, P. Ye, S.L. Kirstein, M.R. Gaylord, S.C. Feinstein, X. Wang, and X. Xu. 2009. Kinetic cell-based morphological screening: prediction of mechanism of compound action and off-target effects. *Chem Biol*. 16:712-723.

Ahmad, S., A. Ahmad, and C.W. White. 2006. Purinergic signaling and kinase activation for survival in pulmonary oxidative stress and disease. *Free Radic Biol Med*. 41:29-40.

Akhtar, M.J., M. Ahamed, S. Kumar, H. Siddiqui, G. Patil, M. Ashquin, and I. Ahmad. 2010. Nanotoxicity of pure silica mediated through oxidant generation rather than glutathione depletion in human lung epithelial cells. *Toxicology*. 276:95-102.

Alberts, B., A. Johnson, J. Lewis, M. Raff, K. Roberts, and P. Walter. 2008. Molecular Biology of the Cell. Garland Science.

Anker, J.N., W.P. Hall, O. Lyandres, N.C. Shah, J. Zhao, and R.P. Van Duyne. 2008. Biosensing with plasmonic nanosensors. *Nat Mater*. 7:442-453.

Asati, A., S. Santra, C. Kaittanis, and J.M. Perez. 2010. Surface-charge-dependent cell localization and cytotoxicity of cerium oxide nanoparticles. *ACS Nano*. 4:5321-5331.

Auffan, M., J. Rose, J.Y. Bottero, G.V. Lowry, J.P. Jolivet, and M.R. Wiesner. 2009. Towards a definition of inorganic nanoparticles from an environmental, health and safety perspective. *Nat Nanotechnol*. 4:634-641.

Baer, D.R., D.J. Gaspar, P. Nachimuthu, S.D. Techane, and D.G. Castner. 2010. Application of surface chemical analysis tools for characterization of nanoparticles. *Anal Bioanal Chem*. 396:983-1002.

Baulig, A., M. Sourdeval, M. Meyer, F. Marano, and A. Baeza-Squiban. 2003. Biological effects of atmospheric particles on human bronchial epithelial cells. Comparison with diesel exhaust particles. *Toxicol In Vitro*. 17:567-573.

Beliatis, M.J., N.A. Martin, E.J. Leming, S.R. Silva, and S.J. Henley. 2011. Laser ablation direct writing of metal nanoparticles for hydrogen and humidity sensors. *Langmuir*. 27:1241-1244.

Berridge, M.J., M.D. Bootman, and P. Lipp. 1998. Calcium--a life and death signal. *Nature*. 395:645-648.

Bhattacharjee, S., L.H. de Haan, N.M. Evers, X. Jiang, A.T. Marcelis, H. Zuilhof, I.M. Rietjens, and G.M. Alink. 2010. Role of surface charge and oxidative stress in cytotoxicity of organic monolayer-coated silicon nanoparticles towards macrophage NR8383 cells. *Part Fibre Toxicol*. 7:25.

Boots, A.W., M. Hristova, D.I. Kasahara, G.R. Haenen, A. Bast, and A. van der Vliet. 2009. ATP-mediated activation of the NADPH oxidase DUOX1 mediates airway epithelial responses to bacterial stimuli. *J Biol Chem*. 284:17858-17867.

Braydich-Stolle, L.K., J.L. Speshock, A. Castle, M. Smith, R.C. Murdock, and S.M. Hussain. 2010. Nanosized aluminum altered immune function. *ACS Nano*. 4:3661-3670.

Breitkreutz, D., V.M. Schoop, N. Mirancea, M. Baur, H.J. Stark, and N.E. Fusenig. 1998. Epidermal differentiation and basement membrane formation by HaCaT cells in surface transplants. *Eur J Cell Biol*. 75:273-286.

Bremer, L., R. Tuinier, and S. Jahromi. 2009. High refractive index nanocomposite fluids for immersion lithography. *Langmuir*. 25:2390-2401.

Byrappa, K., S. Ohara, and T. Adschiri. 2008. Nanoparticles synthesis using supercritical fluid technology - towards biomedical applications. *Adv Drug Deliv Rev*. 60:299-327.

Carvalho, T.C., J.I. Peters, and R.O. Williams, 3rd. 2011. Influence of particle size on regional lung deposition--what evidence is there? *Int J Pharm*. 406:1-10.

Ceresoli, D., Vanderbilt, D. 2006. Structural and dielectric properties of amorphous ZrO2 and HfO2. *Physical Review B*. 74:6.

Cha, K.E., and H. Myung. 2007. Cytotoxic effects of nanoparticles assessed in vitro and in vivo. *J Microbiol Biotechnol*. 17:1573-1578.

Chen, D., and L. Gao. 2004. Novel synthesis of well-dispersed crystalline SnO2 nanoparticles by water-in-oil microemulsion-assisted hydrothermal process. *J Colloid Interface Sci*. 279:137-142.

Cho, W.S., R. Duffin, C.A. Poland, S.E. Howie, W. MacNee, M. Bradley, I.L. Megson, and K. Donaldson. 2010. Metal oxide nanoparticles induce

unique inflammatory footprints in the lung: important implications for nanoparticle testing. *Environ Health Perspect*. 118:1699-1706.

Clift, M.J., S. Bhattacharjee, D.M. Brown, and V. Stone. 2010. The effects of serum on the toxicity of manufactured nanoparticles. *Toxicol Lett*. 198:358-365.

Clogston, J.D., and A.K. Patri. 2011. Zeta potential measurement. *Methods Mol Biol*. 697:63-70.

Cozens, A.L., M.J. Yezzi, K. Kunzelmann, T. Ohrui, L. Chin, K. Eng, W.E. Finkbeiner, J.H. Widdicombe, and D.C. Gruenert. 1994. CFTR expression and chloride secretion in polarized immortal human bronchial epithelial cells. *Am J Respir Cell Mol Biol*. 10:38-47.

Crosera, M., M. Bovenzi, G. Maina, G. Adami, C. Zanette, C. Florio, and F. Filon Larese. 2009. Nanoparticle dermal absorption and toxicity: a review of the literature. *Int Arch Occup Environ Health*. 82:1043-1055.

Dockery, D.W., and C.A. Pope, 3rd. 1994. Acute respiratory effects of particulate air pollution. *Annu Rev Public Health*. 15:107-132.

Donaldson, K., and V. Stone. 2003. Current hypotheses on the mechanisms of toxicity of ultrafine particles. *Ann Ist Super Sanita*. 39:405-410.

EPA, U. 2011. Control of nanoscale materials under the Toxic Substances Control Act.

Fadeel, B., and A.E. Garcia-Bennett. 2010. Better safe than sorry: Understanding the toxicological properties of inorganic nanoparticles manufactured for biomedical applications. *Adv Drug Deliv Rev*. 62:362-374.

Field, J.A., A. Luna-Velasco, S. Boitano, F. Shadman, B.D. Ratner, C. Barnes, and R. Sierra-Alvarez. 2011. Cytotoxicity and physicochemical properties of hafnium oxide nanoparticles. *Chemosphere*.

Grahame, T.J., and R.B. Schlesinger. 2010. Cardiovascular health and particulate vehicular emissions: a critical evaluation of the evidence. *Air Qual Atmos Health*. 3:3-27.

Griffitt, R.J., J. Luo, J. Gao, J.C. Bonzongo, and D.S. Barber. 2008. Effects of particle composition and species on toxicity of metallic nanomaterials in aquatic organisms. *Environ Toxicol Chem*. 27:1972-1978.

Gruenert, D.C., W.E. Finkbeiner, and J.H. Widdicombe. 1995. Culture and transformation of human airway epithelial cells. *Am J Physiol*. 268:L347-360.

Grynkiewicz, G., M. Poenie, and R.Y. Tsien. 1985. A new generation of Ca2+ indicators with greatly improved fluorescence properties. *J Biol Chem*. 260:3440-3450.

Gwinn, M.a.V., V. 2006. Nanoparticles: health effects - pros and cons. *Environmental Health Perspectives*. 114:1818-1825.

Hinderliter, P.M., K.R. Minard, G. Orr, W.B. Chrisler, B.D. Thrall, J.G. Pounds, and J.G. Teeguarden. 2010. ISDD: A computational model of particle sedimentation, diffusion and target cell dosimetry for in vitro toxicity studies. *Part Fibre Toxicol*. 7:36.

Horak, F., Jr., M. Studnicka, C. Gartner, J.D. Spengler, E. Tauber, R. Urbanek, A. Veiter, and T. Frischer. 2002. Particulate matter and lung function growth in children: a 3-yr follow-up study in Austrian schoolchildren. *Eur Respir J*. 19:838-845.

Huang, C.C., R.S. Aronstam, D.R. Chen, and Y.W. Huang. 2010. Oxidative stress, calcium homeostasis, and altered gene expression in human lung epithelial cells exposed to ZnO nanoparticles. *Toxicol In Vitro*. 24:45-55.

Inoue, K. 2011. Promoting effects of nanoparticles/materials on sensitive lung inflammatory diseases. *Environ Health Prev Med*. 16:139-143.

Ju-Nam, Y., and J.R. Lead. 2008. Manufactured nanoparticles: an overview of their chemistry, interactions and potential environmental implications. *Sci Total Environ*. 400:396-414.

Karakoti, A.S., S. Das, S. Thevuthasan, and S. Seal. 2011. PEGylated Inorganic Nanoparticles. *Angew Chem Int Ed Engl*. 50:1980-1994.

Larese, F.F., F. D'Agostin, M. Crosera, G. Adami, N. Renzi, M. Bovenzi, and G. Maina. 2009. Human skin penetration of silver nanoparticles through intact and damaged skin. *Toxicology*. 255:33-37.

Larese Filon, F., M. Crosera, G. Adami, M. Bovenzi, F. Rossi, and G. Maina. 2011. Human skin penetration of gold nanoparticles through intact and damaged skin. *Nanotoxicology*.

Leff, A.R., and P.T. Schumacker. 1993. Respiratory Physiology Basics and Applications. W. B. Saunders Company.

Li, X.Y., P.S. Gilmour, K. Donaldson, and W. MacNee. 1997. In vivo and in vitro proinflammatory effects of particulate air pollution (PM10). *Environ Health Perspect*. 105 Suppl 5:1279-1283.

Lieb, T., C.W. Frei, J.I. Frohock, R.J. Bookman, and M. Salathe. 2002. Prolonged increase in ciliary beat frequency after short-term purinergic stimulation in human airway epithelial cells. *J Physiol*. 538:633-646.

Lommatzsch, M., S. Cicko, T. Muller, M. Lucattelli, K. Bratke, P. Stoll, M. Grimm, T. Durk, G. Zissel, D. Ferrari, F. Di Virgilio, S. Sorichter, G. Lungarella, J.C. Virchow, and M. Idzko. 2010. Extracellular adenosine triphosphate and chronic obstructive pulmonary disease. *Am J Respir Crit Care Med*. 181:928-934.

Marijnissen, J.C.M., and L. Gradoń. 2010. Nanoparticles in Medicine and Environment: Inhalation and Health Effects. Springer.

Mason, H.S., S. Bourke, and P.J. Kemp. 2004. Selective modulation of ligand-gated P2X purinoceptor channels by acute hypoxia is mediated by reactive oxygen species. *Mol Pharmacol*. 66:1525-1535.

Methner, M., L. Hodson, A. Dames, and C. Geraci. 2010. Nanoparticle Emission Assessment Technique (NEAT) for the identification and measurement of potential inhalation exposure to engineered nanomaterials--Part B: Results from 12 field studies. *J Occup Environ Hyg*. 7:163-176.

Muhlfeld, C., P. Gehr, and B. Rothen-Rutishauser. 2008. Translocation and cellular entering mechanisms of nanoparticles in the respiratory tract. *Swiss Med Wkly*. 138:387-391.

Nel, A., T. Xia, L. Madler, and N. Li. 2006. Toxic potential of materials at the nanolevel. *Science*. 311:622-627.

Nel, A.E., L. Madler, D. Velegol, T. Xia, E.M. Hoek, P. Somasundaran, F. Klaessig, V. Castranova, and M. Thompson. 2009. Understanding biophysicochemical interactions at the nano-bio interface. *Nat Mater*. 8:543-557.

Nordberg, G.F., B.A. Fowler, M. Nordberg, and L.T. Friberg. 2007. Handbook on the Toxicology of Metals. Elsevier Inc.

Oberdorster, G. 2010. Safety assessment for nanotechnology and nanomedicine: concepts of nanotoxicology. *J Intern Med*. 267:89-105.

Oberdorster, G., A. Maynard, K. Donaldson, V. Castranova, J. Fitzpatrick, K. Ausman, J. Carter, B. Karn, W. Kreyling, D. Lai, S. Olin, N. Monteiro-Riviere, D. Warheit, and H. Yang. 2005. Principles for characterizing the potential human health effects from exposure to nanomaterials: elements of a screening strategy. *Part Fibre Toxicol.* 2:8.

Pan, Y., S. Neuss, A. Leifert, M. Fischler, F. Wen, U. Simon, G. Schmid, W. Brandau, and W. Jahnen-Dechent. 2007. Size-dependent cytotoxicity of gold nanoparticles. *Small.* 3:1941-1949.

Park, E.J., J. Choi, Y.K. Park, and K. Park. 2008. Oxidative stress induced by cerium oxide nanoparticles in cultured BEAS-2B cells. *Toxicology.* 245:90-100.

Park, S.J., S.W. Lee, K.J. Lee, J.H. Lee, K.D. Kim, J.H. Jeong, and J.H. Choi. 2010. An Antireflective Nanostructure Array Fabricated by Nanosilver Colloidal Lithography on a Silicon Substrate. *Nanoscale Res Lett.* 5:1570-1577.

Peralta-Videa, J.R., L. Zhao, M.L. Lopez-Moreno, G. de la Rosa, J. Hong, and J.L. Gardea-Torresdey. 2011. Nanomaterials and the environment: a review for the biennium 2008-2010. *J Hazard Mater.* 186:1-15.

Samoli, E., P.T. Nastos, A.G. Paliatsos, K. Katsouyanni, and K.N. Priftis. 2011. Acute effects of air pollution on pediatric asthma exacerbation: Evidence of association and effect modification. *Environ Res.*

Sherwood, C.L., R.C. Lantz, J.L. Burgess, and S. Boitano. 2011. Arsenic alters ATP-dependent Ca2+ signaling in human airway epithelial cell wound response. *Toxicol Sci.*

Stone, V., H. Johnston, and R.P. Schins. 2009. Development of in vitro systems for nanotoxicology: methodological considerations. *Crit Rev Toxicol.* 39:613-626.

Teeguarden, J.G., P.M. Hinderliter, G. Orr, B.D. Thrall, and J.G. Pounds. 2007. Particokinetics in vitro: dosimetry considerations for in vitro nanoparticle toxicity assessments. *Toxicol Sci.* 95:300-312.

Thielbeer, F., K. Donaldson, and M. Bradley. 2011. Zeta potential mediated reaction monitoring on nano and microparticles. *Bioconjug Chem.* 22:144-150.

Wang, H.J., A.C. Growcock, T.H. Tang, J. O'Hara, Y.W. Huang, and R.S. Aronstam. 2010. Zinc oxide nanoparticle disruption of store-operated

calcium entry in a muscarinic receptor signaling pathway. *Toxicol In Vitro*. 24:1953-1961.

Warheit, D.B., C.M. Sayes, and K.L. Reed. 2009. Nanoscale and fine zinc oxide particles: can in vitro assays accurately forecast lung hazards following inhalation exposures? *Environ Sci Technol*. 43:7939-7945.

Wiesenthal, A., L. Hunter, S. Wang, J. Wickliffe, and M. Wilkerson. 2011. Nanoparticles: small and mighty. *Int J Dermatol*. 50:247-254.

Wittmaack, K. 2007. In search of the most relevant parameter for quantifying lung inflammatory response to nanoparticle exposure: particle number, surface area, or what? *Environ Health Perspect*. 115:187-194.

Xia, T., M. Kovochich, M. Liong, L. Madler, B. Gilbert, H. Shi, J.I. Yeh, J.I. Zink, and A.E. Nel. 2008. Comparison of the mechanism of toxicity of zinc oxide and cerium oxide nanoparticles based on dissolution and oxidative stress properties. *ACS Nano*. 2:2121-2134.

Zhou, J., J. Ralston, R. Sedev, and D.A. Beattie. 2009. Functionalized gold nanoparticles: synthesis, structure and colloid stability. *J Colloid Interface Sci*. 331:251-262.